ALMA MATER STUDIORUM
UNIVERSITÀ DI BOLOGNA

Dipartimento di Ingegneria Civile, Chimica, Ambientale e dei Materiali - DICAM

Anaerobic Batch Fermentations of C5-C6 Sugars for Acetic Acid Production: A Kinetic Modeling Approach

Tesi di Laurea Magistrale in

Ingegneria Chimica e di Processo

Presentata da:

Panfilia Preda

Relatore:

Prof. Dario Frascari

Correlatore:

Marta Martínez García

Sessione III

Anno Accademico 2023-2024

Abstract

Per promuovere e commercializzare biocarburanti e prodotti chimici di base di nuova generazione, è necessario che essi raggiungano una competitività economica con le alternative derivate da petrolio che intendono sostituire. Tra questi, l'acido acetico si distingue come un acido carbossilico versatile con una vasta gamma di applicazioni in vari settori. Attualmente, la produzione di acido acetico soddisfa le sue richieste attraverso due vie principali: la sintesi chimica e i processi fermentativi aerobici. Quest'ultimo metodo presenta limitazioni intrinseche, poiché la fermentazione aerobica produce, al massimo, 2 moli di acido acetico per mole di glucosio. Al contrario, la via anaerobica che utilizza batteri homoacetogenici offre prospettive più promettenti, con un rendimento teorico massimo di 3 mol/mol. Inoltre, questo approccio presenta minori richieste energetiche, poiché non richiede l'insufflazione di ossigeno. Di conseguenza, l'utilizzo di batteri homoacetogenici per convertire glucosio e xilosio ha attirato notevole attenzione nel contesto della produzione di acido acetico come prodotto chimico di base derivato da fonti rinnovabili, in particolare da idrolizzati lignocellulosici.

Questo lavoro di tesi si concentra su due organismi, *Moorella thermoacetica* e *Thermoanaerobacter kivui*. Inizialmente, la ricerca ha intrapreso analisi separate di ciascun batterio, studiando i rispettivi meccanismi di inibizione da prodotto e da substrato. Successivamente, sono state condotte fermentazioni batch utilizzando zuccheri C5-C6 e, infine, i due organismi sono stati co-coltivati per esplorare potenziali sinergie e ottimizzare gli esiti della fermentazione. Una scoperta degna di nota è stata la necessità di fornire CO_2 esogena per ottenere il completo consumo degli zuccheri. Senza questo supplemento, la WLP rimane inattiva, portando all'inibizione della crescita a causa di un eccesso di NADH. Questa rivelazione sottolinea le complessità coinvolte nel massimizzare l'efficienza della produzione di acido acetico da fonti rinnovabili, aprendo la strada per ulteriori ottimizzazioni e per l'eventuale commercializzazione di questa tecnologia promettente.

Abstract

To promote and commercialize next-generation biofuels and basic chemical products, it is necessary for them to achieve economic competitiveness with the petroleum-derived alternatives they aim to replace. Among these, acetic acid stands out as a versatile carboxylic acid with a wide range of applications in various sectors. Currently, acetic acid production meets its demands through two main pathways: chemical synthesis and aerobic fermentative processes. The latter method has intrinsic limitations since the aerobic fermentation produces, at most, 2 moles of acetic acid per mole of glucose. In contrast, the anaerobic pathway utilizing homoacetogenic bacteria offers more promising prospects, with a maximum theoretical yield of 3 mol/mol. Additionally, this approach has lower energy requirements since it does not require oxygen insufflation. Consequently, the use of homoacetogenic bacteria to convert glucose and xylose has attracted considerable attention in the context of acetic acid production as a basic chemical derived from renewable sources, particularly from lignocellulosic hydrolysates.

This thesis work focuses on two organisms, *Moorella thermoacetica* and *Thermoanaerobacter kivui*. Initially, the research undertook separate analyses of each bacterium, studying their respective product and substrate inhibition mechanisms. Subsequently, batch fermentations were conducted using C5-C6 sugars, and finally, the two organisms were cocultivated to explore potential synergies and optimize fermentation outcomes. A noteworthy discovery was the need to provide exogenous CO_2 to achieve complete sugar consumption. Without this supplement, the WLP remains inactive, leading to growth inhibition due to excess NADH. This revelation underscores the complexities involved in maximizing the efficiency of acetic acid production from renewable sources, paving the way for further optimizations and eventual commercialization of this promising technology.

A Flavia, Gabriele e Luca,

con i quali ho condiviso questa esperienza all'estero.

Non sarebbe stato lo stesso senza di voi.

Contents

List of Figures

List of Tables

Introduction

The current global surge of interest in renewable resources and biorefineries has resulted in a new era of opportunities within the field of biochemical manufacturing. To advance next-generation biofuels and commodity chemicals to a broad commercialization level, bio-based chemical products must establish cost competitiveness with the petroleum-derived alternatives they seek to supplant.

One such bio-based chemical is acetic acid, a versatile carboxylic acid with a wide range of applications across various sectors, including food, pharmaceuticals, chemicals, textiles, polymers, medicine, cosmetics, and more. Acetic acid serves as a fundamental building block with a constantly growing demand. In 2022, the global acetic acid market achieved a remarkable volume, surpassing 17.48 million metric tons (Fig. 1). Projections indicate a further substantial expansion, reaching approximately 23.6 million metric tons worldwide by 2030 [2, 6, 44]. To contextualize this growth, it is noteworthy that the 2022 production of acetic acid represented approximately one-fifteenth of the global market volume of sulfuric acid, the most extensively produced chemical, amounting to 265.05 million metric tons [45].

In terms of utilization, the primary consumption of acetic acid revolves around the production of key derivatives such as vinyl acetate monomer (VAM), acetic anhydride, and C1-C4 acetates. Acetic acid also plays a crucial role as a solvent in the synthesis of terephthalic acid (PET). VAM, a vital component in the polymer industry, serves various functions as an emulsifier, resin, and intermediate in surface coating agents. Additionally, it finds applications in acrylic fibers and polymer wires, contributing significantly to the textile industry through condensation reactions for synthetic fiber production. Acetic anhydride, another derivative, serves as a standard acetylation agent. It is utilized in the production of cellulose acetate, which, in turn, is employed in synthetic textiles and silver-based photographic films. Various esters of acetic acid, including ethyl acetate, n-butyl acetate, isobutyl acetate, and propyl acetate are commonly employed as solvents in inks,

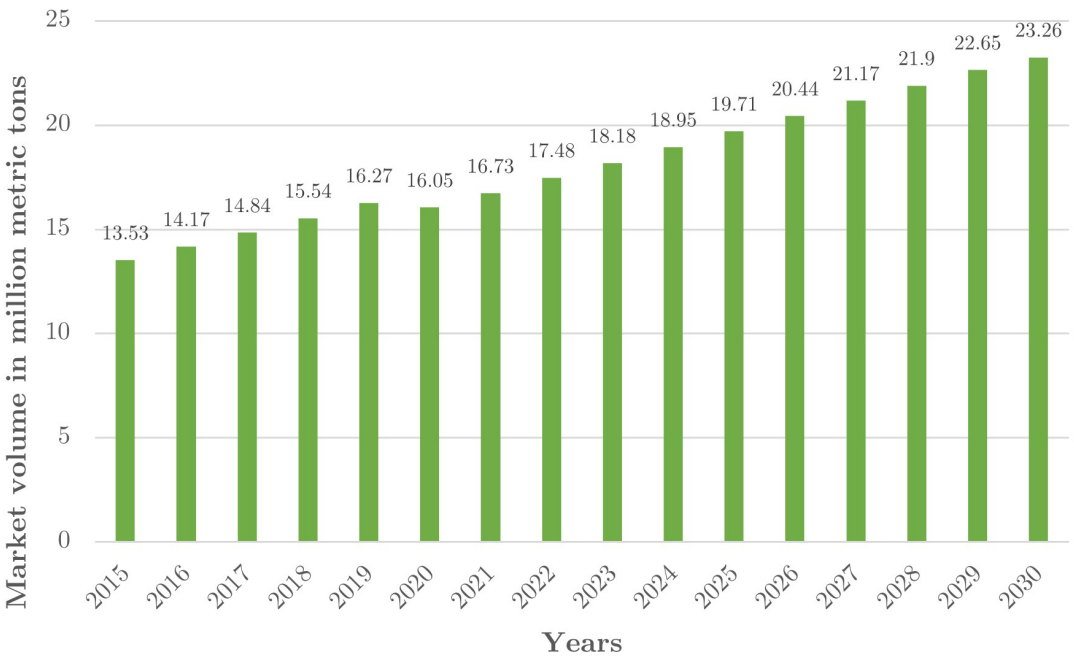

Figure 1: Market volume worldwide from 2015 to 2022, with a forecast from 2023 to 2030 [44].

paints, and coatings. Glacial acetic acid, prized for its excellent polar protic properties, finds frequent use as a solvent for recrystallization in the purification of organic compounds [6].

Currently, acetic acid production meets its demands through two primary routes: chemical and fermentative processes. Chemical manufacturing employs both homogeneous and heterogeneous catalytic methods, with the Cavita process (carbonylation of methanol) standing out as the predominant technique, contributing to over 65% of global acetic acid production [12]. Other significant processes involve the oxidation of aldehyde and ethylene.

On the other hand, acetic acid produced via the fermentation route primarily finds its applications in the food industry, particularly in the form of vinegar. Acetic acid, in varying concentrations, is used to enhance the flavor of foods and prolong their shelf life. New applications have emerged, including edible and non-edible antimicrobial coatings. This process involves utilizing renewable carbon resources like apples, grapes, pears, honey, cane, coconuts, dates, syrups, cereals, and hydrolyzed starch, as well as beer and wine. The fermentation process is typically divided into two stages: first, the treatment with yeast, followed by the involvement of acetic acid bacteria (AAB). Among the various genera of AAB, *Acetobacter*, and *Gluconacetobacter* are the most commonly used. *Acetobacter*

pasteurianus is traditionally used for commercial vinegar production, with concentrations not exceeding 6% (v/v), while *Gluconacetobacter europaeus* is employed to produce high-concentration vinegar (10% v/v). The inherent limitation of this conventional route lies in its theoretical maximum yield, which amounts to 2 moles of acetic acid from 1 mole of glucose or 0.67 g/g glucose. This restriction is attributed to the loss of 2 out of 6 carbon atoms as CO_2 according to the equation:

$$C_6H_{12}O_6 \xrightarrow{S.\ cerevisiae} 2\ C_2H_5OH + 2\ CO_2 \tag{1}$$

$$2\ C_2H_5OH + 2\ O_2 \xrightarrow{A.\ aceti} 2\ CH_3COOH + 2\ H_2O \tag{2}$$

Consequently, one-third of the initial feedstock is lost from an industrial standpoint. Aggravating this challenge is the practical yield of acetic acid in this conventional process, which typically ranges between 0.50-0.55 g/g, accounting for only 75-80% of the theoretical maximum. Furthermore, the method faces additional limitations as it is unable to ferment five-carbon sugars due to the yeast's incapacity to process them, as documented in previous studies [6, 42].

Since the late 1970s, researchers have explored alternative methods for acetic acid production using renewable biomass feedstocks rather than relying on petroleum or natural gas. Simple carbon sources like sugar and starch from crops are considered more suitable, but their primary use as human food and animal feed has raised concerns. As a result, attention has shifted towards non-food crops as substrates, with a recent focus on lignocellulosic biomass as an attractive carbon source. Extensive studies have been conducted on lignocellulosic hydrolysates, as these materials offer the potential to produce a wide range of products, including transportation fuels, commodity chemicals, and chemical precursors for high-value products. Efficiently utilizing these resources is crucial for the development of economically viable bioconversion processes, and organic acid production can benefit from microbial fermentation of lignocellulosic hydrolysates [38]. Lignocellulosic biomass is expected to become the primary source of biomass in the future, being widely available at moderate costs and posing less competition with food and feed production.

Lignocellulosic biomass undergoes pre-treatment to release cellulose, hemicellulose, and lignin, with cellulose being further converted through enzymatic hydrolysis. Glucose and xylose are the most prevalent sugars in lignocellulosic hydrolysates, making up 60-70% and 30-40% of the content, respectively. However, lignocellulosic feedstocks are not as easily converted into simple sugars as starch or molasses and require pre-treatment with acid

catalysts, steam explosion, supercritical water, or enzymes to obtain fermentable sugars. The cost of feedstock and feedstock pre-treatment, which can account for over 50% of the total operating expenditure (OPEX)[32], is a major factor influencing the economic viability of this process. Researchers are actively investigating approaches to achieve complete conversion of these substrates into the desired product, aiming to reduce process costs. To address this challenge, homoacetogenic bacteria, proficient in concurrently metabolizing mixed sugars such as hexoses and pentoses while exclusively yielding acetic acid during fermentation, have been identified and cultivated, offering potential solutions for lignocellulosic biomass valorization.

Compared to acetic acid production via aerobic fermentation, the anaerobic route results in higher acetate yields and has lower energy requirements, as it does not require oxygen aeration. As a result, the homoacetogenic conversion of glucose and xylose has garnered attention in the context of acetic acid production as a feedstock chemical produced from renewable resources. To fully capitalize on all available sugars, it is crucial to employ microorganisms with the capacity to convert both hexose and pentose carbohydrates efficiently. This adaptability is vital for the effective and economical utilization of lignocellulosic hydrolysates [13, 21, 38].

This thesis will primarily delve into homoacetogenic fermentations focusing on C5 and C6 sugars. The central organisms of interest for these experiments are *Moorella thermoacetica* and *Thermoanaerobacter kivui*. These bacteria have been chosen because they are particularly appealing from an industrial standpoint due to their carbon conversion efficiency. Additionally, their anaerobic and thermophilic nature holds promise for potentially reducing fermentation costs compared to more common aerobic fermentation methods. In fact, they present a lower susceptibility to contamination, heightened metabolic and diffusion rates, reduced cooling expenses, and potentially diminished costs associated with product recovery [36].

The research aims to investigate the following aspects:

- Assessing product inhibition for each strain to determine the threshold concentration of acetic acid that induces growth inhibition.
- Investigating substrate inhibition for each strain to identify the optimal initial substrate concentration that maximizes growth rate without impeding growth.
- Conducting batch fermentation for each strain using their preferred carbon sources.

- Exploring the potential synergies and enhanced fermentation outcomes through co-culturing of the two organisms.

These findings are necessary for advancing to various fermentation methodologies, with a particular emphasis on continuous fermentations. Continuous processes would enable the application of this innovative approach to industrial-scale operations for the production of acetic acid.

Chapter 1

Homoacetogenesis

To gain a comprehensive understanding of the experiments under scrutiny in this thesis, it proves advantageous to furnish a succinct yet comprehensive overview of the landscape of homoacetogenic bacteria, commonly known as "acetogenic bacteria", at the commencement of this study.

Acetogenesis boasts a rich historical background reaching as far back as the early 20th century. In 1932, Fischer and his team made a groundbreaking discovery when they observed the production of acetate within sewage sludge through this process. Nonetheless, it wasn't until 1936 that Dutch microbiologist K.T. Wieringa successfully isolated the very first acetogen, which he named *Clostridium aceticum*. This mesophilic, spore-forming bacterium was located in ditch mud. Regrettably, cultures of *C. aceticum* were lost for several decades until German microbiologist G. Gottschalk stumbled upon a vial of *C. aceticum* spores in the collection of H.A. Barker. These spores were utilized to reestablish the microorganism for further research. In 1942, a second thermophilic, spore-forming acetogen, initially named *Clostridium thermoaceticum* and later renamed *Moorella thermoacetica*, was isolated from horse manure by F.E. Fontaine [10].

Acetogens play a crucial role in the biology of various ecosystems, including soil, lakes, oceans, animal gastrointestinal tracts, termites, rice paddy soils, hypersaline waters, surface soils, and deep subsurface sediments, which typically share the trait of having very low oxygen concentrations. Their presence extends to unexpected realms, as evidenced by their identification in methanogenic mixed populations within diverse settings, including an army ammunition manufacturing plant wastewater treatment facility and a dechlorinating community intentionally enriched for bioremediation purposes. This widespread distribution underscores the adaptability of acetogens, capable of thriving both autotrophically

on H_2, CO_2, and CO, and heterotrophically by metabolizing an array of substrates such as hexoses, pentoses, alcohols, and acids [34, 41]. In these varied environments, acetogens directly compete with hydrogenotrophic methanogenic archaea or engage in syntrophic interactions with acetotrophic methanogens.

Similar to methanogens, some acetogens serve as a sink for H_2, depleting hydrogen generated in anaerobic settings during the natural biodegradation of organic compounds. Despite the dominance of methanogens as primary hydrogenotrophs in many ecosystems due to their lower H_2 threshold and greater energy yield from converting CO_2 and H_2 into methane compared to acetate, acetogens exhibit versatility in their metabolic pathways for growth. This adaptability is vital for their survival, allowing them to thrive in environments where alternative strategies are required, showcasing the complexity and resilience of their metabolic capabilities [18, 34].

1.1 Autotrophy

Acetogens can utilize gaseous substrates by employing the acetyl-CoA pathway to fix carbon dioxide (CO_2) using reducing equivalents, such as hydrogen (H_2), for the synthesis of acetyl-CoA. This characteristic pathway is known as the Wood–Ljungdahl pathway (WLP). The WLP (Fig. 1.1) is a linear pathway featuring two converging branches responsible for reducing and merging two CO_2 molecules, ultimately yielding one molecule of acetyl-CoA. These branches are the methyl branch and the carbonyl branch.

In the methyl branch, CO_2 is reduced to formate through formate dehydrogenase (FDH). Formate is then bound to tetrahydrofolate to create 10-formyltetrahydrofolate, which undergoes subsequent reduction and dehydration reactions to produce 5-methyltetrahydrofolate, serving as the precursor for the methyl group of acetyl-CoA. In the carbonyl branch, a second CO_2 molecule is reduced to enzyme-bound carbon monoxide (CO), which acts as the precursor for the carbonyl group of acetyl-CoA. This reaction is catalyzed by the key enzyme of the WLP, carbon monoxide dehydrogenase/acetyl-CoA synthase (CODH/Acs), which also facilitates the synthesis of acetyl-CoA from the methyl group, CO, and coenzyme A through an enzymatic mechanism involving several organometallic intermediates.

Before this reaction, the methyl group is transferred from the cofactor tetrahydrofolate to CODH/Acs by a corrinoid-containing methyltransferase. The resulting product, acetyl-CoA, can be integrated into biomass or converted into end products, such as acetate.

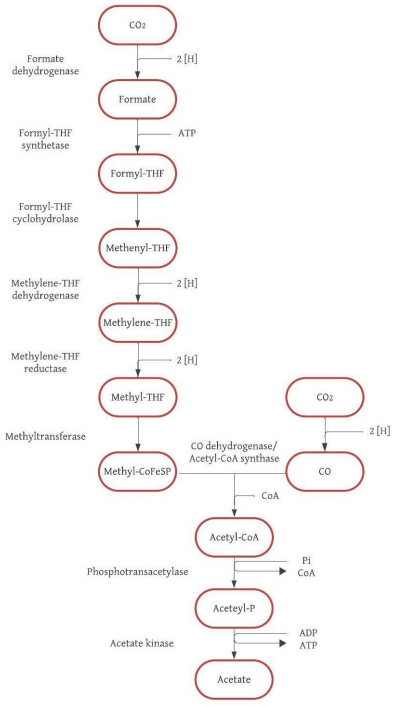

Figure 1.1: The Wood-Ljungdahl pathway of acetogenic bacteria.

It is important to note that essential enzymes in the acetyl-CoA pathway rely on metal ions. Carbon monoxide dehydrogenase requires Ni, formate dehydrogenase relies on Se, Wo, Mo, and Fe, and the corrinoid-protein is dependent on Co. Hence, trace elements hold considerable importance for acetogenic bacteria [21].

Among all biological CO_2 fixation pathways, the WLP stands out as the most efficient in terms of energetic requirements. Only one ATP and four reducing equivalents, such as NAD(P)H, are used in this reaction. To balance the ATP-consuming step, which involves the fusion of formate to the cofactor tetrahydrofolate, acetic acid is produced through substrate-level phosphorylation (SLP), generating ATP. As a result, there is no net gain of ATP in the complete pathway [14, 18, 28]. Acetogenic growth in autotrophic environments is thus exclusively reliant on chemiosmotic energy-conserving mechanisms that are connected to the translocation of protons or sodium ions.

1.2 Heterotrophy

Although acetogens demonstrate their ability to thrive in laboratory conditions with H_2 and CO_2 as substrates, this reaction does not appear to be their primary reliance in their natural environments due to the typically low H_2 concentrations. In anoxic settings, the

concentration of H_2 generally ranges from 0.01 to 0.04 mbar, while acetogens require a minimum threshold of around 0.43–0.95 mbar for efficient CO_2 utilization [18]. Additionally, autotrophic growth, as observed in acetogens, is not highly competitive in natural ecosystems, especially when compared to methanogens. Therefore, it does not fully account for the widespread distribution of acetogens.

Carbohydrates such as glucose can provide more energy than the sole WLP if converted to incompletely oxidized end products, such as ethanol, lactate, or acetate, by fermentation.

Through glycolysis via the Embden-Meyerhof-Parnas pathway (EMP), one mole of hexose (e.g., glucose) can be converted to two moles of pyruvate, two moles of ATP, and four electrons. This is the most commonly used central metabolic pathway among the facultative and strict anaerobic chemoheterotrophic bacteria.

The two pyruvate molecules are then transformed into acetyl-CoA, leading to the production of acetic acid and the release of two moles of CO_2 and four additional electrons per mole of glucose (Eq. 1.1).

$$C_6H_{12}O_6 + 2\ H_2O \rightarrow 2\ CH_3COOH + 2\ CO_2 + 8\ [H] \tag{1.1}$$

So overall, glycolysis yields 2 mol of acetyl-coA, 2 mol of ATP, 2 mol of CO_2, and eight electrons from each mole of glucose.

1.3 Mixotrophy

Acetogenic mixotrophy or anaerobic, non-photosynthetic mixotrophy, stands out as a distinctive feature of acetogens, rendering them particularly intriguing when compared to other fermentative bacteria. This trait becomes pivotal in overcoming the constraints inherent in autotrophic growth and addressing the CO_2 loss linked to hetereotrohpic growth.

In mixotrophy, carbon fixation into product occurs through both the glycolytic pathway and the WLP. The surplus ATP generated by glycolysis supports the fixation of CO_2 through the WLP, thus facilitating the generation of one additional acetyl-CoA and optimizing carbon yield (Fig. 1.2) [14, 28, 34, 39].

Lacking a mechanism for the reabsorption of CO_2, carbon dioxide produced through glycolysis would be lost, and a significant portion of the pool of reducing equivalents would be oxidized through hydrogenase activity, leading to the release of H_2 [14]. However, acetogens, distinctively among fermentative organisms, have the ability to recycle the excess reducing equivalents in the form of two NADH and two molecules of ferredoxin (Fd_{red}) by

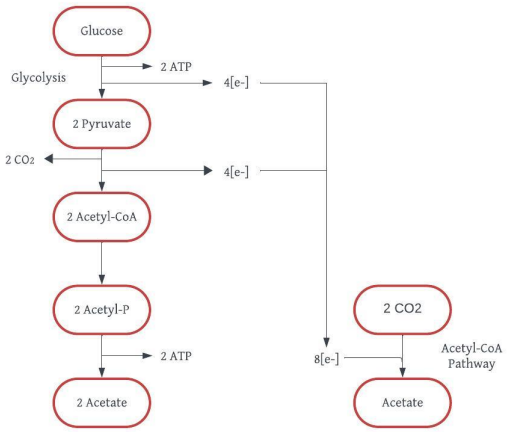

Figure 1.2: Homoacetogenic conversion of glucose to acetate.

reducing two CO_2 molecules through the WLP (Eq. 1.2).

$$2\ CO_2 + 8\ [H] \rightarrow CH_3COOH + 2\ H_2O \tag{1.2}$$

Overall, the homoacetogenic conversion of glucose leads to the production of three acetate molecules, as outlined in Equation 1.3 [30]:

$$C_6H_{12}O_6 \rightarrow 3\ CH_3COOH \tag{1.3}$$

During autotrophic growth, one key role of the WLP is to fix CO_2 for biomass formation, while in the context of mixotrophic growth, the WLP takes on a critical function in energy conservation. Every chemotrophic organism derives energy from the oxidation of an energy-rich substrate and must subsequently reoxidize the reduced electron carriers to maintain a balanced redox stoichiometry. This can be accomplished by either transferring the electrons to an external electron acceptor, like oxygen, or, in the case of fermentations, directing them toward an incompletely oxidized intermediate.

Glycolysis and the WLP work in tandem since the two molecules of CO_2 and eight electrons generated through glycolysis can be fully harnessed by the WLP, enabling the reoxidation of the reduced electron carriers and yielding an additional acetyl-CoA. This results in a 50% increase in acetyl-CoA yield compared to the standard EMP glycolysis [14].

The reoxidation of reducing equivalents by the WLP not only replenishes the cell's electron carriers but also allows further substrate oxidation, liberating additional energy that the cell can effectively utilize. Consequently, the thermodynamic favorability of mixotrophic growth over autotrophic and heterotrophic growth becomes evident, leading to a more efficient conservation of ATP in the cellular processes.

Homoacetogenic fermentation illustrates the modular nature of acetogenic metabolism. The first module encompasses the electron-donating reactions, while the second module links the recycling of redox cofactors to energy conservation. Finally, the third module represents the terminal electron-accepting pathway. When commencing with hexose, the process can achieve a maximum theoretical yield of 3 mol/mol, rendering it particularly compelling from an industrial perspective.

However, as in many fermentation processes for chemical production, the accumulation of the end product inhibits cell growth and further product formation. Product inhibition generally increases with increasing concentrations of the product. A major obstacle in the development of bioprocesses is to attain a high volume-specific productivity while maintaining a high concentration of inhibitory products. The end product of homoacetogenic fermentation, acetic acid, is inhibitory to cell growth mainly in the undissociated form (acetic acid), but also in the ionized form (acetate).

Acetogens exhibit sensitivity to acetate and acidic conditions primarily due to the disruption of proton motive force and transmembrane electrical potential, as highlighted in previous studies [10]. The characteristic pH difference between the intracellular and extracellular environments plays a crucial role, with observations demonstrating that organisms like *Moorella thermoacetica* maintain an intracellular pH approximately 0.6 units more alkaline than the extracellular pH in batch cultures. Weak organic acids, such as acetic acid, function as uncoupling agents, diminishing this essential pH disparity.

As acetic acid passively diffuses through the bacterial cytoplasmic membrane, increasing concentrations in the medium are mirrored by rising concentrations within the cell. However, as long as a ΔpH is maintained, the intracellular concentration of anion plus acid surpasses the extracellular concentration. Equation 1.4 illustrates that, for instance, to sustain a ΔpH of 0.6, the intracellular acetate concentration would need to attain 2 M when cells are cultivated in an external acetate environment of 0.5 M.

$$\Delta pH = log \frac{[Ac^-]_{in}}{[Ac^-]_{out}} \tag{1.4}$$

Unfortunately, these elevated internal acetate concentrations, hinder some of the key the enzymes involved in acetate synthesis. For instance, enzyme inhibition studies with cell-free extracts of *T. kivui* revealed that pyruvate ferredoxin-oxidoreductase's activity was inhibited by 50% with 1.2 M sodium acetate, while the concentration inhibiting acetate kinase by 50% was 0.84 M. Consequently, high acetate concentrations impede enzymes responsible for converting pyruvate to acetyl-CoA and acetyl-phosphate to acetate [21].

As discussed thus far, carbon dioxide holds particular significance in the acetyl coenzyme A pathway, and many acetogens cannot achieve optimal growth under either heterotrophic or autotrophic conditions in the absence of exogenous CO_2. Even though exogenous CO_2 is not necessary for the stoichiometry of mixotrophy, sugars are frequently not used to their full potential without it. This phenomenon may arise due to oxidative processes that occur before pyruvate is decarboxylated during glycolysis producing CO_2. As a result, sufficient exogenous CO_2 is frequently required for the recycling of electron carriers [10].

Some acetogens, such as *A. woodii*, present an exceptionally high carbonic anhydrase (CA) specific activity. CA is a zinc-containing enzyme, which catalyzes the following reaction (Eq. 1.5):

$$CO_2 + H_2O \leftrightarrow HCO_3^- + H^+ \tag{1.5}$$

One of its physiological functions in acetogens might involve raising intracellular CO_2 levels. Since acetogens produce substantial amounts of acetic acid during growth, CA could also play a role in regulating intracellular pH.

However, in the case of thermophilic acetogens, where the equilibrium between CO_2 and HCO_3^- is reached more rapidly due to the higher temperatures, this enzyme may not have a significant physiological role. It is believed that environmental factors such as temperature, pH, and the availability of CO_2 - HCO_3^- might influence the physiological role of CA in acetogens [4].

It is essential to discuss the significance of oxygen concentration levels in addition to carbon dioxide. Acetogens are considered obligatory anaerobes, if not strictly so. *Strict* anaerobes are killed by oxygen, in contrast to *obligatory* anaerobes, which are unable to use molecular oxygen but may withstand varying amounts of oxygen in the atmosphere. More than 5 μM of dissolved oxygen prevent strictly anaerobic bacteria from growing because some of the key acetogenesis-related enzymes are very sensitive to O_2. As a strong oxidizing agent, oxygen can undergo radical reactions that produce superoxides, peroxides, and hydroxyl radicals when it comes into contact with light or a transition metal like iron, manganese, or cobalt. Sensitive biomolecules may then become oxidized by these reactive oxygen radicals [10, 41].

Acetogens have been discovered, nevertheless, in environments where redox stability is subject to fluctuations. Well-aerated soils and the root zones of salt marsh and estuarine macrophytes, which occasionally encounter oxygen-enriched conditions, are home to a

sizable population of cultivable acetogens. In these redox-unstable situations, acetogens probably need to adapt to cope with periods of oxidative stress. Since the first acetogen, *C. aceticum*, was isolated from soil that was likely subjected to intermittent wetting and drying (aeration), it is not surprising that recent investigations have shown a variety of adaptive mechanisms utilized by acetogens to manage oxidative stress in situ. These adaptive mechanisms include:

- *Reductive Elimination of O_2* Acetogens contain a range of enzymes that can be used to reductively eliminate oxygen and its dangerous byproducts, such as superoxide and peroxide. These enzymes include reduced nicotinamide adenine dinucleotide (NADH) oxidase, rubredoxin oxidoreductase (a superoxide reductase), rubrerythrin (a peroxidase), catalase, cytochrome bd oxidase, and superoxide dismutase. In situations when oxygen concentrations are low, these enzymes are especially effective in shielding acetogens from oxidative destruction.

- *Using Different Electron Acceptors in Response to O_2* When it comes to choosing terminal electron acceptors, acetogens are flexible. Because of this, some acetogens can divert the flow of reducing equivalents from the acetyl-CoA pathway to less oxygen-sensitive terminal electron-accepting pathways. These other processes operate at higher redox potentials than the acetyl-CoA pathway. A representative case may be found in *M. thermoacetica*, where the nitrate/nitrite half-cell reaction's greater standard redox potential (430 mV) suggests that nitrate dissimilation is less oxygen-sensitive than acetogenesis.

- *Trophic Interaction with Partners Who Consume Oxygen* Acetogens can coexist symbiotically with microaerophiles that consume oxygen and aerotolerant fermenters. It has been demonstrated that interactions between the microaerophilic bacterium *Thermicanus aegyptius* and the acetogen *M. thermoacetica* occur; the two species were initially co-cultured from Egyptian soil. In general, the fermentative non-acetogen consumes oxygen to make fermentation products (such formate, lactate, and H_2) that the acetogen can use for acetogenesis, protecting it from oxygen exposure [10].

The redox potential (ORP or Eh), which is related to both the reducing potential of the culture medium and the availability of oxygen, is another important factor for anaerobic bacteria. If the medium's redox potential is too high, anaerobic bacteria may not be able to proliferate, which frequently calls for the use of reducing chemicals.

After completing the overview on the metabolic routes leading to anaerobic acetate production, the next subsections will describe the acetogenic species employed in this work.

1.4 *Moorella thermoacetica*

Moorella thermoacetica stands out as an exceptionally versatile homoacetogen, showcasing a remarkable degree of metabolic diversity. This gram-positive, thermophilic, and anaerobic bacterium, formerly named *Clostridium thermoaceticum*, thrives optimally at temperatures between 55–60°C and at a pH of 6.8.

A defining feature of *M. thermoacetica* lies in its unique metabolic capabilities. As a homoacetogen, it adeptly transforms various sugars, including xylose, fructose, and glucose, into acetic acid. The conversion of glucose (Eq. 1.6) and fructose follows the Embden–Meyerhof–Parnas glycolytic pathway, while xylose undergoes processing through the pentose phosphate pathway (PPP) (Eq. 1.7). The genome of *M. thermoacetica* encodes all enzymes essential for these pathways [12, 34].

$$C_6H_{12}O_6 \rightarrow 3\,CH_3COOH \tag{1.6}$$

$$2\,C_5H_{10}O_5 \rightarrow 5\,CH_3COOH \tag{1.7}$$

Furthermore, like all acetogens, this bacterium exhibits the ability to synthesize acetic acid from carbon dioxide, employing the WLP. This metabolic flexibility positions *M. thermoacetica* as a robust competitor for substrates in diverse environments. Apart from its metabolic versatility, *M. thermoacetica* possesses survival strategies that contribute to its resilience. Notably, its spores display exceptional heat resistance, with a decimal reduction time of up to 111 minutes at 121°C. Additionally, the bacterium's nutritional requirements are minimal, with nicotinic acid being the sole essential component for NAD conversion [9, 27, 34].

When considering heterotrophic growth on monosaccharides, *M. thermoacetica* is reported to have a particular form of carbon catabolite repression (CCR) by preferentially consuming xylose over glucose [2, 12], unlike most bacteria. Despite being the preferred carbon source, xylose uptake is slow. However, with subsequent transfers in a medium containing only xylose as carbon source, the rate of utilization of this substrate can be increased [2]. Additionally, the bacterium's capacity to produce acetic acid is influenced

by the presence of metals, which stimulate fermentation rates and formate dehydrogenase activity [1].

Drake and Daniel [9] reported that, when *M. thermoacetica* is cultivated on glucose, 31% of the labeled [^{14}C]glucose is recovered as $^{14}CO_2$/carbonates, 62% as [^{14}C]acetate, and 6% as [^{14}C]biomass. Consequently, in heterotrophic cultures, the generation of carbon dioxide persists even when the initial gas phase is 100% CO_2. However, a higher production of CO_2, resulting from glycolysis but not utilized by the WLP, leading to lower yields, is observed in environments lacking CO_2 enrichment, such as with 100% N_2 [9, 20]. The dependence on exogenous CO_2 becomes then evident as *M. thermoacetica* faces growth challenges in its absence. This suggests that environments enriched with CO_2, maintaining this electron acceptor at levels approaching physiological saturation, are crucial for efficient acetate production.

1.5 *Thermoanaerobacter kivui*

In 1981 Leigh et al. [25] isolated the homoacetogenic bacterium *Thermoanaerobacter kivui* from the sediments of Lake Kivu, to which it owes its name. The organism is a gram-negative, obligate anaerobic, non-motile, non-spore-forming rod that measures approximately 0.7 μm in width and 2-7.5 μm in length. It is frequently found in pairs or chains. It grows in a temperature range between 50 and 72 °C but its optimum is 66°C, being therefore the most thermophilic acetogenic bacterium characterized so far. As for pH, its optimum is 6.4 but it grows in an interval between 5.3 and 7.3 [3, 25].

In comparison to other non-acetogenic species in the *Thermoanaerobacter* genus as well as other acetogens, *T. kivui*'s substrate range is quite limited. For example, unlike *M. thermoacetica*, *T. kivui* is not able to metabolize alcohols, and unlike mesophilic *Sporomusa* species or *A. woodii*, it cannot use methylated compounds such as methanol, methylamines, or glycine betaine. It has been reported that other than H_2 + CO_2 and CO, *T. kivui* solely uses pyruvate, formate, and the sugars glucose, fructose, and mannose to create acetate. [3, 4, 13]. *T.kivui* does not have any vitamin requirements but has a high demand for trace elements [3, 21].

While the carbonic anhydrase activity in *T. kivui*, and in thermophilic acetogens in general, is minimal, the presence of exogenous CO_2 has been shown to influence growth. It has been demonstrated that the CO_2 released from sugar oxidation is sufficient to sustain growth, albeit at significantly reduced rates. Indeed, when *T. kivui* is grown on glucose in

an HCO_3^- (and CO_2)-free medium, the doubling time increases, and growth is slowed down. Without HCO_3^-, cells grown on glucose also produce slightly less acetate than with HCO_3^-, and some H_2 is produced. This indicates that *T. kivui* utilizes protons as electron acceptors in the absence of CO_2, presumably via the electron-bifurcating hydrogenase, working in the confurcating direction. However, despite utilizing additional electron acceptors during growth when compelled to do so, the WLP remains the major electron sink. The removal of H^+ through proton reduction is not rapid enough to match the growth rate [30].

Chapter 2

Materials and methods

2.1 Bacterial strains and growth medium

The strains of *Moorella thermoacetica* (DSM 2955) and *Thermoanaerobacter kivui* (DSM 2030) were obtained from the German Collection of Microorganisms (DSMZ) as lyophilized pellets and subsequently revived in growth medium DSM 60 supplemented with glucose and DSM 171 supplemented with H_2/CO_2, respectively. In order to enhance xylose utilization by *M. thermoacetica*, the cells underwent four sequential transfers in medium containing xylose as the sole C source. Taking into consideration the intention to co-culture both strains in the future, *T. kivui* was also grown on DSM 60. For preservation of both strains, cells in mid-exponential growth phase were used to prepare cryostocks in 10% v/v DMSO and stored at -80°C.

DSM 60 growth medium (see Table 2.1), was formulated from six distinct solutions sterilized separately at 121°C for 20 minutes. To complete the medium, solutions B to F were added sequentially to Solution A in a sterile, anaerobic manner immediately before inoculation. The composition of solutions A to F is detailed in Table 2.2, with quantities specified per liter of solution.

2.2 Bacth cultivation in serum vials tests

Solution A was prepared, and aliquots of the desired volume were dispensed into 160 mL serum bottles. These bottles were sealed with a butyl rubber plug and crimp cap, and sparged for 10 minutes with 100% CO_2. Subsequently, the headspace of the bottles was exchanged with 100% CO_2, applying an overpressure of 200 mbar, to establish anaerobic conditions before autoclaving.

Table 2.1: Composition of DSM 60 medium.

Solution A	843.00	mL
Solution B	50.00	mL
Solution C	50.00	mL
Solution D	40.00	mL
Solution E	10.00	mL
Solution F	10.00	mL

Table 2.2: Composition of the solutions of DSM 60 medium.

Solution A	$MgSO_4$	0.10	g
	$(NH_4)_2SO_4$	0.50	g
	$Fe(NH_4)_2(SO_4)_2$	0.04	g
	$Na_2MoO_4 \times 2\ H_2O$ (0.1 % w/v)	2.40	mL
	$Na_2SeO_3 \times 5\ H_2O$ (0.1% w/v)	0.15	mL
	Tryptone	5.00	g
	Yeast extract	5.00	g
	Sodium resazurin (0.1% w/v)	0.50	mL
	Distilled water	840.00	mL
Solution B	K_2HPO_4	7.00	g
	KH_2PO_4	4.50	g
	Distilled water	50.00	mL
Solution C	Glucose	12.00	g
	Xylose	6.00	g
	Distilled water	50.00	mL
Solution D	Na_2CO_3	2.00	g
	Distilled water	40.00	mL
Solution E	L-Cysteine HCl $\times$ H_2O	0.30	g
	Distilled water	10.00	mL
Solution F	$Na_2S \times 9\ H_2O$	0.30	g
	Distilled water	10.00	mL

Solutions B, C, D, E, and F were prepared in individual serum bottles sealed with a butyl rubber plug and crimp cap. To create anaerobic environments, the bottles were flushed with 100% N_2 gas and the headspace exchanged to 100% N_2, except for Solution D, which was under an 80% N_2 and 20% CO_2 gas atmosphere. After autoclaving, all the solutions were stored at room temperature on the laboratory bench, for use in subsequent experiments.

Complete DSM 60 medium was prepared by adding the required quantity of Solutions B-F to Solution A under sterile and anaerobic conditions. These were achieved by transferring all volumes with syringes and needles previously flushed with N_2 and working in a laminar flow hood (for sterility) in close proximity to a flame (for anaerobiosis). The pH of the complete medium was adjusted to approximately 6.9 with 1.5 mL of 1M NaOH.

Subsequently, precultures were inoculated with 1.5 mL of DMSO cryo-cultures and incubated for 24 hours in a New Brunswick Innova®42 shaking incubator, maintained at 58°C and 175 rpm for experiments involving *M. thermoacetica* and 60°C for experiments with *T. kivui*. These precultures served as the inoculum for the actual cultures, targeting an initial OD of 0.2. Bacterial growth was monitored during the tests, and the optical density (OD) of cells was measured at 600 nm using a Shimadzu™ UV-1800 Spectrophotometer, while pH was concurrently measured using WTW pH/Ion 340i Meter.

2.2.1 Product inhibition test

Both strains were cultivated in crimp-capped serum bottles (160 mL nominal volume) using DSM 60 medium, supplemented with glucose (18 g/L), and varying concentrations of sodium acetate trihydrate (0 M, 0.10 M, 0.19 M, 0.29 M, 0.39 M, 0.48 M, 0.58 M, and 0.68 M). Sodium acetate was added to the medium before inoculation to simulate the acetate produced by acetic acid dissociation.

At a given pH, the concentrations of acetic acid and acetate can be calculated using the Henderson-Hasselbalch equation (Eq. 2.6). Considering the dissociation reaction of acetic acid, AcH:

$$AcH \leftrightarrow H^+ + Ac^- \tag{2.1}$$

The equilibrium constant (k_{eq}) is determined as:

$$k_{eq} = \frac{k_f}{k_r} = \frac{[H^+][Ac^-]}{[AcH]} \tag{2.2}$$

Where k_f and k_r are the fractional rates constants for the forward and reverse reaction and [AcH], [Ac^-] and [H^+] represent the concentrations in moles per liter. Because this

is the constant for acid dissociation, it is also referred to as the acid constant (K_a). The negative $\log_{10}$ of the K_a is indicated as the pK_a:

$$pK_a = -log\Big(\frac{[H^+][Ac^-]}{[AcH]}\Big) \tag{2.3}$$

$$pK_a = -log\Big(\frac{[Ac^-]}{[AcH]}\Big) - log[H^+] \tag{2.4}$$

$$pK_a = -log\Big(\frac{[Ac^-]}{[AcH]}\Big) + pH \tag{2.5}$$

$$pH = pK_a + log\Big(\frac{[Ac^-]}{[AcH]}\Big) \tag{2.6}$$

Rearranging provides for the Henderson-Hasselbalch equation (Eq. 2.6). The pK_a is therefore the pH at which the acid is half-dissociated when in equilibrium [23].

2.2.2 Substrate inhibition tests

Crimp-capped serum bottles (160 mL nominal volume) containing 50 mL of DSM 60 medium and varying concentrations of total substrate were employed.

To assess the impact of different sugar concentrations, four distinct levels were examined in duplicate trials (9 g/L, 18 g/L, 36 g/L, and 54 g/L). For *Moorella thermoacetica*, two sets of tests were conducted. In the first set, only xylose was used. In the second set of tests, glucose and xylose were used in a 2:1 mass ratio. For *Thermanaerobacter kivui*, the study focused on the impact of glucose alone.

2.2.3 Co-culture

Crimp-capped serum bottles (nominal volume 160 mL) with 50 mL of DSM 60 growth medium containing glucose (9 g/L) and xylose (9 g/L xylose). The inoculation process involved introducing precultures cultivated on glucose for *T. kivui* and xylose for *M. thermoacetica*. To establish an initial OD_{600} of 0.2, the appropriate volume of the precultures was added, ensuring an equal contribution of 0.1 for each strain.

2.2.4 Co-culture supplemented with DMSO

Crimp-capped serum bottles (nominal volume 160 mL) with 50 mL of DSM 60 growth medium, containing glucose and xylose in a 2:1 mass ratio. The total concentration of these sugars was 12 g/L for glucose and 6 g/L for xylose. The inoculation procedure mirrored that of the preceding co-culture experiment. However, after 24 and 45 hours, 2.5

mL of anaerobic dimethyl sulfoxide (DMSO) 2 M were introduced into the cultures. In addition, 2 mL of sterile and anaerobic NaOH 1 M were added after 23 and 45 hours.

2.3 Fermentation

All fermentation experiments were conducted in a 3 L Applikon fermenter with a working volume of 1.5 L under strict anaerobic conditions. The fermenter was equipped with a pH sensor, a redox sensor, and a pressure sensor to facilitate comprehensive monitoring.

Solution A was prepared and autoclaved directly within the fermenter, initially in aerobic conditions. Subsequently, Solutions B and C were introduced aerobically using a peristaltic pump. Continuous sparging with 100% CO_2 was employed to achieve anaerobiosis after this addition. While still under continuous CO_2 flushing, Solution D was added using a peristaltic pump. Finally, solutions E and F (containing the reducing agents to bring redox value down to -300 mV) were introduced through a septum on the top plate of the fermenter, using a sterile syringe flushed with N_2, in order to minimize any contact with air.

The fermenter was inoculated with precultures grown on xylose for *Moorella thermoacetica* and on glucose for *Thermoanaerobacter kivui*, aiming for an initial OD_{600} of 0.2. Before inoculation, precultures grown in serum bottles were transferred to a sterile and anaerobic Schott-Duran bottle inside an anerobic chamber under N_2 atmosphere. From this bottle, the preculture was inoculated into the fermenter using a peristaltic pump operating at 50 rpm.

All fermentations were conducted using the same DSM 60 medium employed in the batch serum vial tests. *Moorella thermoacetica* underwent two fermentation processes, one exclusively on xylose, and the other supplemented with glucose and xylose in a 2:1 mass ratio. Meanwhile, *Thermoanaerobacter kivui*'s fermentation was provided with glucose only. The medium for *M. thermoacetica* fermentations included 2 g/L of Na_2CO_3 following the original recipe, whereas *T. kivui*'s fermentation contained 10 g/L of $NaHCO_3$. Another modification from the original recipe is observed in the fermentations involving *T. kivui* and *M. thermoacetica* on xylose only, where the concentration of $(NH_4)_2SO_4$ was increased to 1 g/L. This adjustment was made based on prior tests, which indicated a rapid depletion of NH_4-N.

All fermentations were performed at 55°C with continuous agitation at 300 rpm. pH was maintained by using an 5 M NaOH solution, to ensure minimal impact on the culture

volume. The pH setpoint was maintained at 6.8 for *M. thermoacetica* when utilizing xylose exclusively. For *T. kivui*'s fermentation and *M. thermoacetica*'s one with glucose and xylose in a 2:1 mass ratio, the pH setpoint was adjusted to 6.4.

The fermentation involving *M. thermoacetica* utilizing glucose and xylose took place at atmospheric pressure, with CO_2 being purged at a rate of 2 L/min after 20 hours, reaching a total volume of 6.06 L. In contrast, the other two fermentations were conducted under overpressure conditions. A pressure control loop initiated CO_2 flushing when the pressure sensor detected a value below the setpoint of 150 mbar. For *T. kivui*'s fermentation, the condenser outlet was connected to a back pressure valve designed to open when the overpressure exceeded 200 mbar, preventing flow for lower overpressure values. This additional safety measure aimed to enhance overall safety, as to not rely solely on the pressure release valve. Unfortunately, the flow could not be halted even when the fermenter pressure was below the setpoint. Consequently, the condenser outlet was closed during working hours, while it remained open during the night due to pressure increases resulting from the $NaHCO_3$ - CO_2 equilibrium. As a result, between 5 and 22 hours and 31 and 46 hours after inoculation, the overpressure stabilized at around 110 mbar, and the pressure control loop continuously sparged CO_2 at a rate of 5 L/min. In the fermentation involving *M. thermoacetica* on xylose, where sodium bicarbonate was not used, it was safe to close the fermentation outlet, and the overpressure was attained without CO_2 flushing.

Bacterial growth was monitored during fermentations by measuring optical density at 600 nm. Samples of 11 mL were collected right after inoculation and at specific intervals thereafter. Ten milliliters of aliquots were centrifuged at 9000 rpm for 5 minutes at 4°C to separate microbial cells and supernatant. The supernatant underwent filtration using a 0.2 μm syringe filter and was then stored at -20°C for subsequent analysis of sugar, ammonium nitrogen and acetic acid. The cell pellet was washed with deionized water and lyophilized for dry cell weight measurements.

2.4 Analysis

2.4.1 Monomeric sugars

The concentrations of glucose and xylose were determined using High Performance Anion Exchange Chromatography with Pulsed Amperometric Detection (HPAEC-PAD). Thermo Scientific Dionex ICS-5000 ion chromatography system was used at 25°C with milli-Q water, 250 mM NaOH, and 1 M NaOAc as the mobile phase at a flow rate of 1 mL/min.

2.4.2 Acids

The concentrations of acetic acid, ethanol, and formic acid were analyzed using High Performance Liquid Chromatography coupled with a Refractive Index Detector (HPLC-RID+UV). Agilent 1200 Series was used at 60°C with 0.01 M H_2SO_4 as the mobile phase at a flow rate of 0.8 mL/min.

2.4.3 Ammonium-Nitrogen

Ammonium-N concentrations were determined using HACH®LCK303 cuvettes, and a HACH®DR3900 Spectrophotometer, following the protocol provided by the manufacturer. The measuring range was between 2 and 47 mg/L of ammonium-N.

2.4.4 Headspace composition

Gas composition (GC) measurements were conducted by extracting 1 mL of headspace and analyzing it using the Thermo Scientific TRACE GC Ultra with two channels. The analysis was performed employing helium as the carrier gas with a flow rate set at 5.0 mL/min. The column and detector temperatures were 60 and 160°C, respectively.

Chapter 3

Acetic acid production by *M. thermoacetica*

3.1 Product inhibition test

The impact of increasing concentrations of acetate on the specific growth rate of *Moorella thermoacetica* was investigated in batch cultivation in a serum vial. The optical density and pH were measured at different time-points of the growth curve (Fig. 3.1). Cell growth came to a complete halt at a critical product concentration for growth, P_m, despite the presence of sufficient nutrients.

The complete inhibition of growth was observed when employing a solution containing 0.58 M sodium acetate, equivalent to 34.3 g/L of acetate. This maximum concentration is lower than the value reported by Wang and Wang [47] for *Moorella thermoacetica*. In their study, total growth inhibition occurred at concentrations between 0.04 and 0.05 M (approximately 2.79 g/L) due to undissociated acetic acid, while the maximum acetate achievable in the ion concentration was 0.80 M (48 g/L). As it is often the case with undissociated acids, *Moorella thermoacetica* shows greater sensitivity to acetic acid as opposed to acetate. Below pH 6.0, 2.7 g/L of undissociated acetic acid is reached before attaining an acetate concentration of 48 g/L. While above pH 6.0, the inhibitory concentration of acetate is reached before attaining the maximum inhibitory undissociated acetic acid concentration.

However, even at the lowest acetate concentrations tested, there was a discernible impact on growth, leading to a reduced maximum OD_{600}. Samples containing sodium acetate not only exhibited diminished growth, but the growth curve also displayed a temporal shift

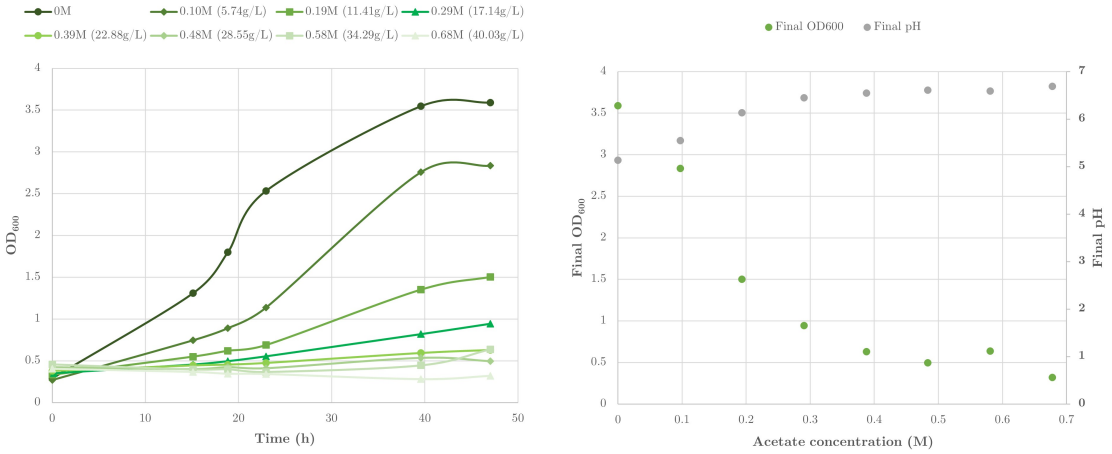

(a) **(b)**

Figure 3.1: Effect of initial increasing acetate concentrations on OD_{600} **(a)** and final OD_{600} and pH **(b)** for *M. thermoacetica*.

after inoculation when compared to the control sample. To support this, Schwartz and Keller [40] observed a dramatic difference in the mass doubling time of *M. thermoacetica* when acetic acid was initially added. A t_d of approximately 6 h at pH 6.0 and 7.0 without added acetic acid was reported, and it increased to about 18 h at pH 6.0 and an initial acetic acid concentration of 1.25%.

The final pH (Fig. 3.1b) decreased as the initial sodium acetate concentration decreased because at low initial sodium acetate concentrations, cell growth was less inhibited. As a consequence, acetic acid was produced at higher concentrations, which probably exceeded the buffering capacity of the sodium carbonate and made the pH of the medium decrease.

The specific growth rate was determined during the exponential phase using the formula:

$$\mu = \frac{\Delta ln OD_{600}}{\Delta t} \tag{3.1}$$

The results depicted in Figure 3.2 demonstrate that the introduction of sodium acetate to the medium indeed hampers the growth of *M. thermoacetica*, leading to a reduction in the specific growth rate. The decline from $\mu = \mu_0$ (for P= 0) to $\mu = 0$ (for P = P_m) can be characterized by Equation 3.2 using a simple linear model [46, 47].

$$\mu = \mu_0 \left(1 - \frac{P}{P_m}\right) \tag{3.2}$$

Originally proposed by Ghose and Tyagi in 1979, this equation finds mathematical analogy in the work of Dagley and Hinshelwood dating back to 1938.

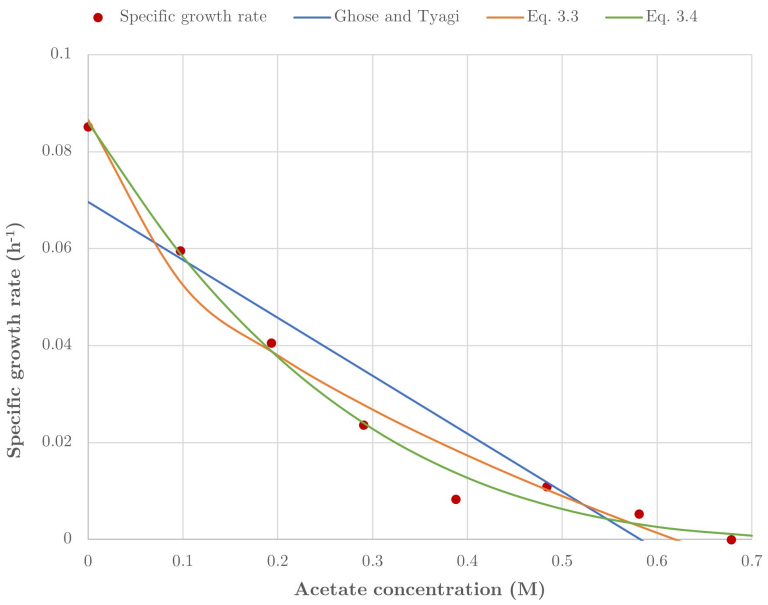

Figure 3.2: Dependence of maximum specific growth rate on acetate concentration according to Eq. 3.2-3.4 for *M. thermoacetica*.

The Mean Squared Error (MSE) method was used to determine the maximum product concentration that leads to complete growth inhibition. In order to do so, experimental data was fitted minimizing the MSE using the Solver add-in function in Microsoft Excel work spreadsheet. The resulting μ_0 and P_m values are reported in Table 3.1. However, the Ghose-Tyagi model fails to accurately represent the observed results (Fig. 3.2), as evidenced by the low coefficient of determination.

Despite its historical roots, deviations between the linear model and experimental data have prompted the exploration of alternative equations.

Two notable extensions of Equation 3.2 introduce an additional parameter, the exponent n_P. While the Ghose-Tyagi model results in a straight line in a plot of μ_{max} vs. P, Eq. 3.3 and 3.4 may better accommodate data points with positive or negative curvature.

$$\mu = \mu_0\left(1 - \left(\frac{P}{P_m}\right)^{n_P}\right) \tag{3.3}$$

$$\mu = \mu_0\left(1 - \frac{P}{P_m}\right)^{n_P} \tag{3.4}$$

Applying the MSE method once more to calculate μ_0, P_m and n_P for Eq. 3.3, this adjustment results in a closer alignment between the model and experimental data (Fig. 3.2), as reflected by a higher R^2 value. Above all, Eq. 3.4 emerges as the superior choice for approximation, exhibiting the highest R^2 value. In this case, the optimal parameter

Table 3.1: Models used for prediction of product inhibition and their estimated parameters for *M. thermoacetica*.

Model	Equation	Parameters	MSE	R^2
Ghose-Tyagi	$\mu = \mu_0\left(1 - \frac{P}{P_m}\right)$	$\mu_0 = 0.07$ h^{-1} $P_m = 0.58$ M	$9.89{\cdot}10^{-5}$	0.88
Eq. 3.3	$\mu = \mu_0\left(1 - \left(\frac{P}{P_m}\right)^{n_P}\right)$	$\mu_0 = 0.09$ h^{-1} $P_m = 0.62$ M $n_P = 0.51$	$2.42{\cdot}10^{-5}$	0.97
Eq. 3.4	$\mu = \mu_0\left(1 - \frac{P}{P_m}\right)^{n_P}$	$\mu_0 = 0.09 \pm 0.01^a$ h^{-1} $P_m = 0.95 \pm 0.08$ M $n_P = 3.48 \pm 0.46$	$6.16{\cdot}10^{-6}$	0.99

[a] Best fit estimate ± 95% confidence interval [43].

for P_m is higher than the value measured experimentally, but aligns more closely to the maximum product concentration reported by Wang and Wang [47].

Additionally, exponential and hyperbolic inhibition models exist, described by Eqs. 3.5 and 3.6, which utilize only $K_{i,p}$ as the inhibition parameter. However, these models are suitable only at relatively low product concentrations. Moreover, they lack a critical product concentration at which growth halts, making them unsuitable for modeling product inhibition when high product concentrations are involved [46]. Due to these considerations, they were excluded as potential mathematical models for the gathered experimental data.

$$\mu = \mu_0 \exp\left(\frac{P}{K_{i,P}}\right) \tag{3.5}$$

$$\mu = \mu_0\left(\frac{K_{i,P}}{K_{i,P} + P}\right) \tag{3.6}$$

3.2 Substrate inhibition

3.2.1 Substrate inhibition test on xylose

A serum vial test was conducted to assess the influence of increasing xylose concentrations (ranging from 9 to 54 g/L) on the specific growth rates of *Moorella thermoacetica*. Throughout the experiment, monitoring included measurements of optical density (OD_{600}) and pH, xylose and acetic acid concentrations. The results, derived from duplicate measurements, are depicted in Figure 3.3.

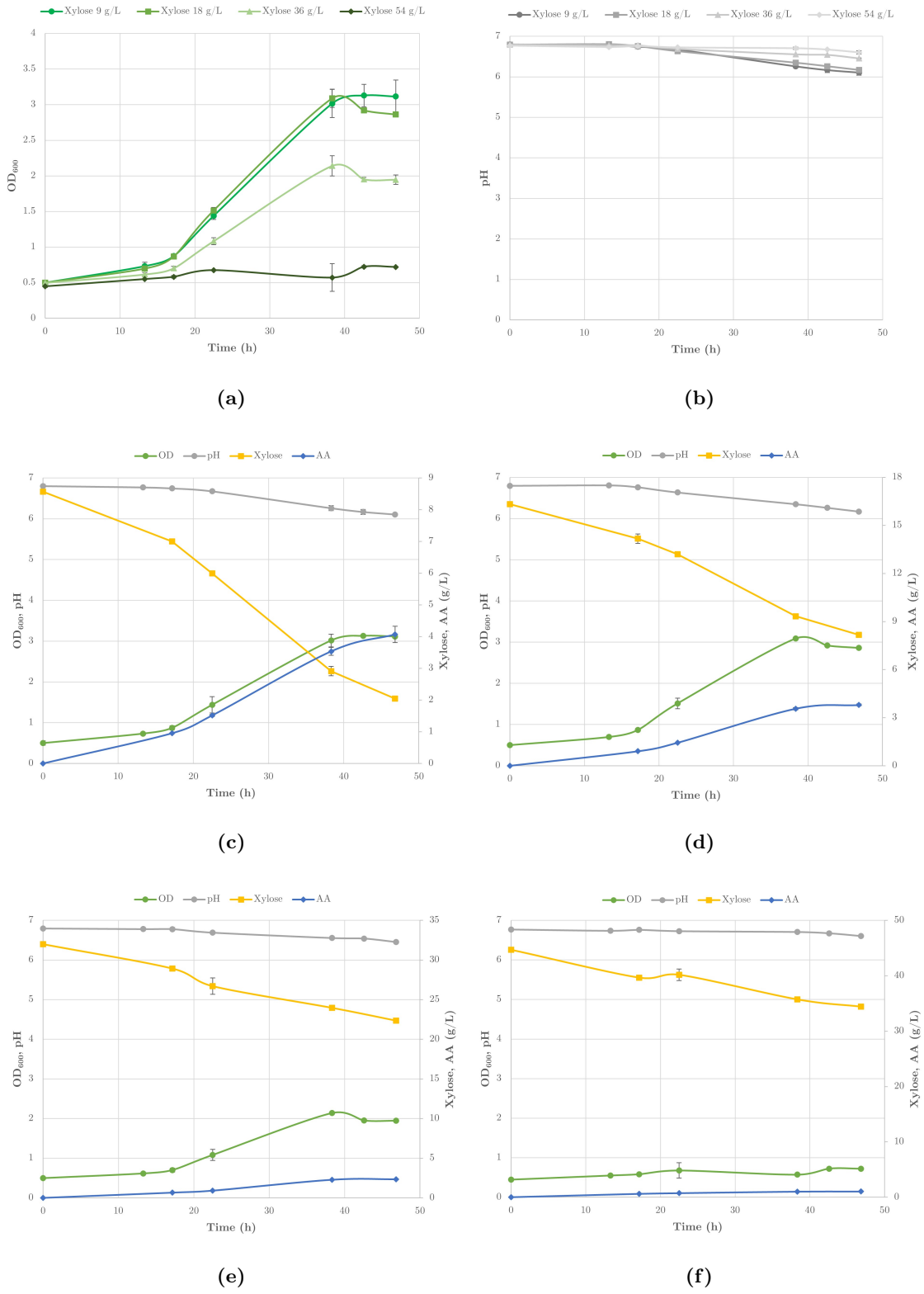

Figure 3.3: Evolution of **(a)** OD_{600}, **(b)** pH, xylose, and acetic acid in cultures of *M. thermoacetica* at increasing xylose concentrations: **(c)** 9 g/L, **(d)** 18 g/L, **(e)** 36 g/L, and **(f)** 54 g/L.

A xylose concentration of 54 g/L resulted in complete growth inhibition. Additionally, cultures with 36 g/L displayed susceptibility to the increasing xylose concentration, exhibiting lower ODs compared to cultures with 9 and 18 g/L (Fig. 3.3a). This observation indicates a discernible impact on growth dynamics as xylose concentrations increase.

The pH levels for all tested conditions decreased to approximately 6 (Fig. 3.3b), a range that deviates from the optimum for *M. thermoacetica*. However, this shift should not be considered inhibitory, as *M. thermoacetica* is known to tolerate variations from its optimal pH range (between 5.7 – 7.7) [9].

The final acetic acid concentration is inversely proportional to the initial sugar concentration. Cultures with 9 g/L of xylose exhibit a higher acetic acid concentration of 4.07 g/L, followed by 3.80 g/L of for cultures with 18 g/L of xylose. Cultures with 36 g/L of xylose produce less acetic acid (2.36 g/L), as expected given the lower OD reached, while those with 54 g/L, showing negligible growth, titer only 1.05 g/L. The concentrations of acetate and undissociated acetic acid were calculated using the Henderson-Hasselbalch equation (see Section 2.2.1 in Materials and Methods), and were both found to be below inhibitory thresholds (0.8 M and 0.04 M for acetate and acetic acid respectively according to Wang and Wang [47]).

Therefore, the growth arrest noted after 38 hours should not be attributed to either the final product concentration or pH inhibition. An insightful addition could have been measuring xylulose accumulation in the culture. *M. thermoacetica* metabolizes xylose through the isomerase pathway, converting xylose into xylulose, and then phosphorylating it to xylulose-5-phosphate, which then enters the pentose phosphate pathway (PPP) [8]. Balasubramanian et al. [2] observed an accumulation of this intermediate in their batch fermentation, which could indicate an impediment to complete the metabolism of this pentose. The conversion of xylulose to xylulose- 5- phosphate requires ATP, so a deficiency in energy supply might be the cause for the incomplete pathway.

The yield of acetic acid was calculated based on both the consumed and the initial xylose concentrations (Fig.3.4). The yield calculated on initial xylose showed a decline as substrate concentration increased, as a consequence of the greater fraction of sugar that remained unused by the bacteria. Surprisingly, this decrease in yield persisted even when calculating it based on the xylose consumed and the obtained values were notably lower than the theoretical maximum acetic acid yield of 2.5 mol/mol associated with xylose growth.

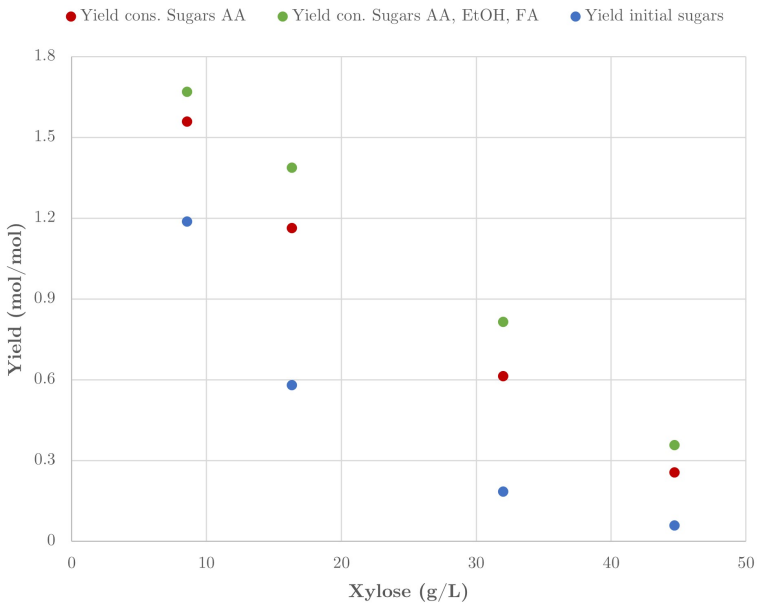

Figure 3.4: Product yields in cultures of *M. thermoacetica* with different xylose concentrations. **(Red markers)** acetic acid yield on consumed xylose; **(Blue markers)** acetic acid yield on initial xylose; **(Green marker)** product yield (including acetic acid, formic acid and methanol) on consumed xylose.

Beyond biomass production, a fraction of the carbon substrate was utilized for ethanol and formic acid production. Low concentrations of ethanol were measured (0.03 g/L, 0.02 g/L, 0.04 g/L, and 0 g/L, respectively). While formic acid shows an increasing trend (0.19 g/L, 0.53 g/L, 0.59 g/L, and 0.32 g/L, for each concentration). According to Drake and Daniel [9], ethanol may be produced at trace levels under excess reductant conditions, as described in Eq. 3.7 [14], where a reducing agent is required to convert Acetyl-CoA to ethanol.

$$Acetyl - CoA + 2\ NAD(P)H \rightarrow Ethanol \tag{3.7}$$

Formic acid is an intermediate in the WLP and its accumulation suggests a halted pathway. As mentioned in the previous Chapter, formate is produced in the methyl branch of the WLP by reducing CO_2 through formate dehydrogenase (FDH). Subsequentially, an ATP-dependent formate-tetrahydrofolate ligase binds formate to tetrahydrofolate to form 10-formyltetrahydrofolate. The formic acid concentrations in the samples may result from insufficient ATP or the use of reducing agents for other reactions, such as ethanol and hydrogen production. In fact, the hydrogenase enzyme, responsible for hydrogen consumption, may also produce H_2 under certain conditions, diverting electrons from the WLP

to protons. According to Kellum and Drake [20], *M. thermoacetica* may boost hydrogenase production in response to sub-optimal heterotrophic conditions. Thus, higher sugar concentrations inducing growth inhibition might lead to increased hydrogen production. This could be checked by performing headspace analysis of the cultures to measure H_2 production.

However, even considering the total moles of products (acetic acid, ethanol, and formic acid) divided by moles of consumed xylose, the yield exhibited a decreasing trend (Fig. 3.4). So, while by-products contribute to a lower yield than the theoretical maximum, they do not entirely explain the observed decrease with increasing initial sugar concentration.

The specific growth rate was determined during the exponential phase using Equation 3.1. The highest specific growth rate observed was 0.104 h^{-1}, occurring with a xylose concentration of 18 g/L. In contrast, cultures containing 54 g/L displayed a negligible specific growth rate (Fig. 3.5). This decline at higher substrate concentrations is attributed to substrate inhibition. Bacteria typically employ active transport mechanisms for sugar and nutrient uptake, facilitated by carrier proteins, which display specific inhibition, substrate specificity, and saturability properties [8]. This adds a layer of complexity to the biochemical dynamics, necessitating more sophisticated models to accurately describe bacterial growth [26].

The Monod model, introduced by Jacques Monod in 1942, serves as a mathematical analogue to the Michaelis–Menten expression for enzyme kinetics. The model is expressed by Eq. 3.8:

$$\mu = \mu_{max} \frac{S}{K_S + S} \tag{3.8}$$

where μ_{max} represents the maximum specific growth rate of cells (h^{-1}), S is the substrate concentration in g/L, and K_S is the substrate saturation constant (g/L), indicating the concentration at which the specific growth rate is half of the maximum ($\mu = 1/2\ \mu_{max}$) [29].

While the Monod model is a simple and mechanistic approach, it has five notable limitations. These include assumptions regarding the independence of the maximum specific growth rate from substrate concentration at high levels, dependence on substrate concentration at low levels, inapplicability in the presence of substrate inhibition, neglect of substrate needs during the stationary phase, and omission of lag and death phases [31]. To address these limitations, particularly in cultures with high substrate concentrations, various models in the literature offer solutions that account for substrate inhibition.

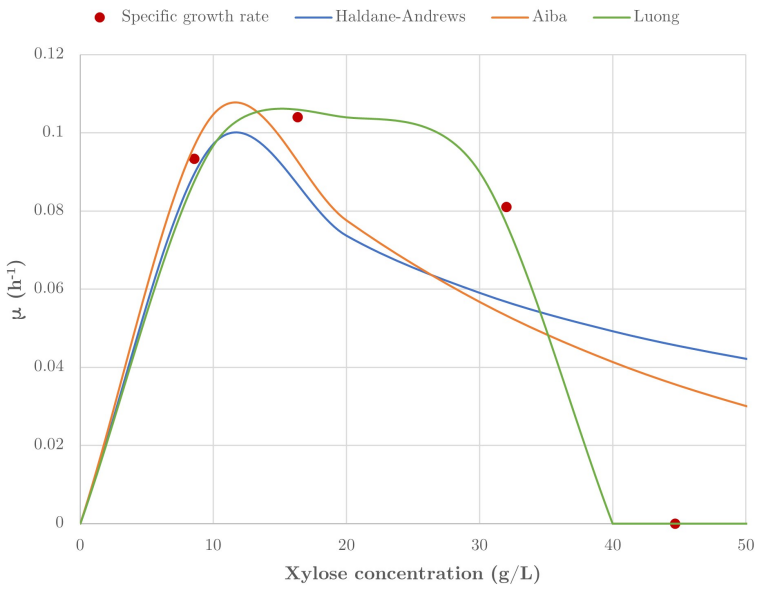

Figure 3.5: Dependence of maximum specific growth rate on substrate concentration according to Haldane-Andrews, Aiba-Edward, and Luong models for *M. thermoacetica*.

One such model is the Haldane-Andrews model (Eq. 3.9), introduced in 1930. This model, an extension of the Monod model, introduces a third constant, K_i, accounting for specific growth rate inhibition at both low and high substrate concentrations. K_i, measured in g/L, indicates the highest substrate concentration at which the specific growth rate equals half of the maximum growth rate in the absence of inhibition [5, 17, 31, 33].

$$\mu = \mu_{max} \frac{S}{K_S + S + \frac{S^2}{K_i}} \tag{3.9}$$

Despite experimental data fitting and parameter estimation minimizing the MSE, the Haldane-Andrews model failed to accurately represent the observed results (Fig. 3.5), as indicated by a low coefficient of determination. The resulting μ_{max}, K_S, and K_i values are reported in Table 3.2.

Another model under consideration is the Aiba-Edward model (Eq. 3.10), proposed by Aiba in 1968, and later adapted by Edward in 1970. This model introduces an inhibitory constant (K_i) and an exponential ratio involving substrate concentration and the inhibitory constant, addressing toxic substrate concentrations within the bioreactor [31, 33].

$$\mu = \frac{\mu_{max} S}{K_s + S} \exp\left(-\frac{S}{K_i}\right) \tag{3.10}$$

Table 3.2: Models used for prediction of xylose inhibition and their estimated parameters for *M. thermoacetica*.

Model	Equation	Parameters	MSE	R^2
Haldane - Andrews	$\mu = \mu_{max}\frac{S}{K_S+S+\frac{S^2}{K_i}}$	$\mu_{max} = 0.15$ h^{-1} $K_S = 0.34$ g/L $K_i = 19.63$ g/L	$3.26 \cdot 10^{-3}$	0.65
Aiba - Edward	$\mu = \frac{\mu_{max}S}{K_s+S}\exp\left(-\frac{S}{K_i}\right)$	$\mu_{max} = 0.15$ h^{-1} $K_S = 0.39$ g/L $K_i = 31.32$ g/L	$5.15 \cdot 10^{-4}$	0.76
Luong	$\mu = \frac{\mu_{max}S}{K_s+S}\left(1-\frac{S}{S_m}\right)^{n_S}$	$\mu_{max} = 0.15 \pm 0.003$ h^{-1} $K_S = 4.17 \pm 0.17$ g/L $S_m = 33.98 \pm 2.57$ g/L $n_S = 0.16 \pm 0.08$	$4.47 \cdot 10^{-15}$	1.00

The Aiba-Edward model yielded only a modest improvement in R^2 values (Table 3.2), still far from accurately representing the experimental data.

So, despite the strengths of the Haldane-Andrews and Aiba-Edward models in comprehensively describing all growth phases, including lag and death phases, they are unable to accurately represent the empirical values observed in this study.

Finally, the Luong model (Eq. 3.11), introduced by Luong in 1987, was applied. This unstructured model characterizes kinetic growth rates based solely on substrate concentration and it is another extension of the Monod equation.

$$\mu = \frac{\mu_{max}S}{K_s+S}\left(1-\frac{S}{S_m}\right)^{n_S} \tag{3.11}$$

This model introduces a novel term to capture complete growth inhibition beyond a critical substrate concentration. Sharing the same structure as Eq. 3.4, which proved optimal for describing product inhibition in this strain, the model effectively predicts the substrate threshold, S_m, at which growth becomes inhibited. Remarkably, this model achieved an R^2 value of 1, indicating an excellent fit to the experimental data.

By minimizing the MSE for Luong's model, the maximum specific growth rate on xylose of *M. thermoacetica* was determined to be 0.15 h^{-1}. This aligns with the specific growth rate of 0.15 ± 0.2 h^{-1} reported by Schmitt et al. [38] during a batch fermentation on 20 g/L of xylose. Furthermore, a value of K_S of 2.30 ± 1.34 g/L was reported, closely

resembling the value obtained through the current model. Their study, however, did not account for a maximum substrate concentration, while the present model estimates it to be 33.98 g/L. Additionally, according to Luong model, operating with xylose concentrations ranging from approximately 12 to 26 g/L would yield the highest specific growth rates.

3.2.2 Substrate inhibition test on glucose and xylose

As the ultimate objective is to utilize lignocellulosic streams as carbon source for acetate production, which typically feature diverse sugar compositions rather than being solely comprised of xylose, a serum vial test was conducted to evaluate the impact of increasing glucose and xylose concentrations (ranging from 9 to 54 g/L) on the specific growth rates of *Moorella thermoacetica*. The choice of using hexose and pentose sugars in a 2:1 mass ratio was guided by Ehsanipour et al. [12], who emphasized the substantial impact of sugar ratios on acetic acid yield.

Throughout the experiment, the optical density (OD_{600}) and pH were monitored. The results, averaged from duplicate measurements, are illustrated in Fig. 3.6a and 3.6b. As it can be observed, none of the sugar concentrations led to complete growth inhibition. Cultures with 9 g/L of sugars exhibited the lowest OD_{600}, while those with 54 g/L reached the highest optical density, despite an initial delay. The pH for all conditions dropped to values around 5.5, a potential inhibitory range for growth. This was compensated by correction with NaOH 1 M after 43 hours, which resulted in a slight resurgence in growth.

According to Andreesen et al. [1] and Balasubramanian et al. [2], in a medium containing a mixture of glucose and xylose, *M. thermoacetica* ferments xylose first. The consumption of the hexose starts when about half of the xylose is fermented. However, in this experiment glucose and xylose appeared to be consumed simultaneously for all conditions tested (Fig. 3.6c - 3.6f). It is noteworthy that, for a total substrate concentration of 9 g/L and 18 g/L, growth tended to peak concurrently with the depletion of the pentose sugar.

Acetic acid concentrations did not reflect the substantial difference in initial substrate concentrations. The final concentrations ranged from a minimum of 6.38 g/L for the culture with 9 g/L of total sugars to a maximum of 7.90 g/L for the culture with 54 g/L of total sugars. Concentrations of acetate and undissociated acetic acid for every condition were determined using the Henderson-Hasselbalch equation. Undissociated acetic acid was in concentrations ranging from 0.043 M to 0.069 M, which represent inhibitory levels,

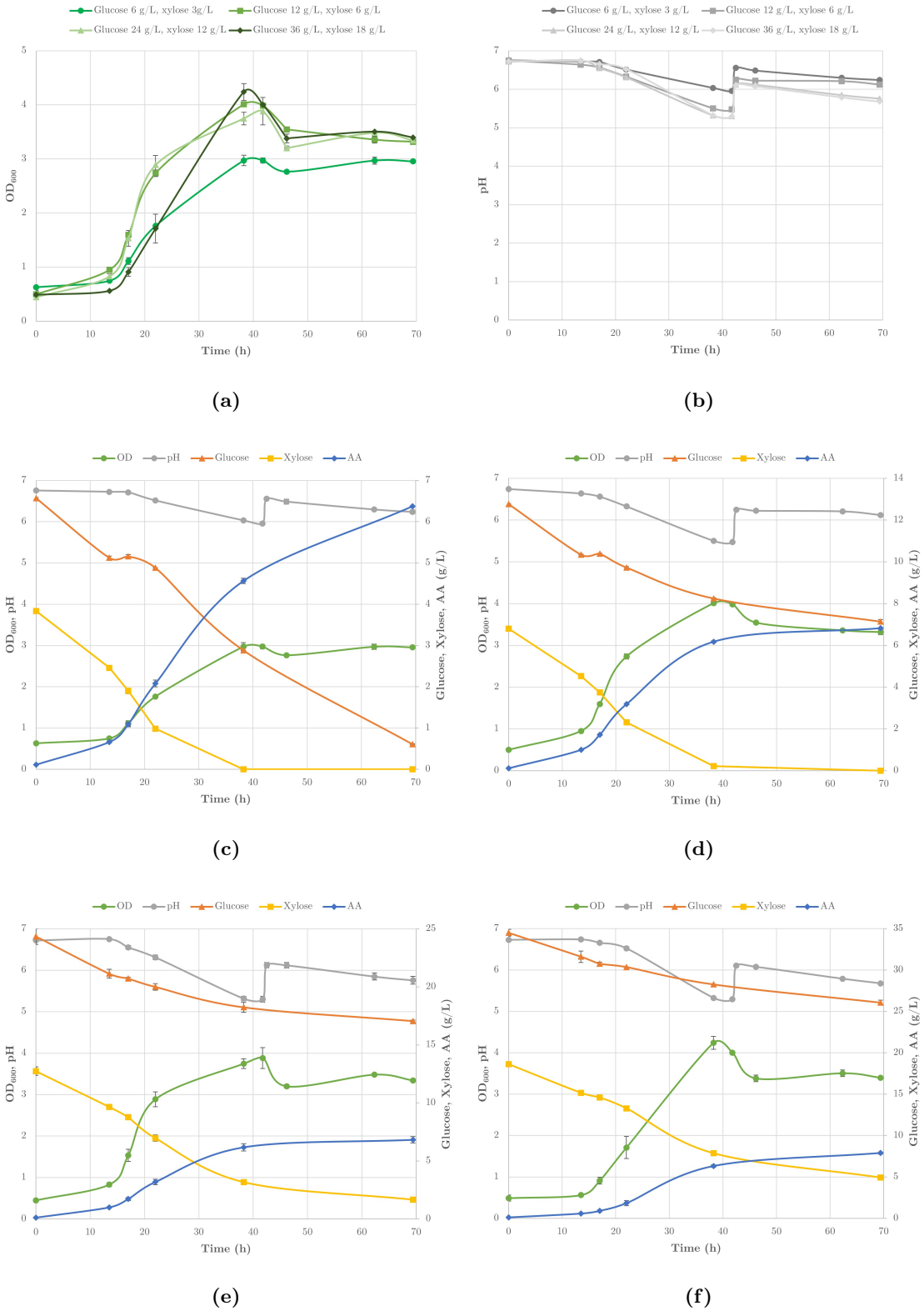

Figure 3.6: Evolution of **(a)** OD_{600}, **(b)** pH, glucose, xylose, and acetic acid in cultures of *M. thermoacetica* at increasing sugar concentrations: **(c)** 9 g/L, **(d)** 18 g/L, **(e)** 36 g/L, and **(f)** 54 g/L.

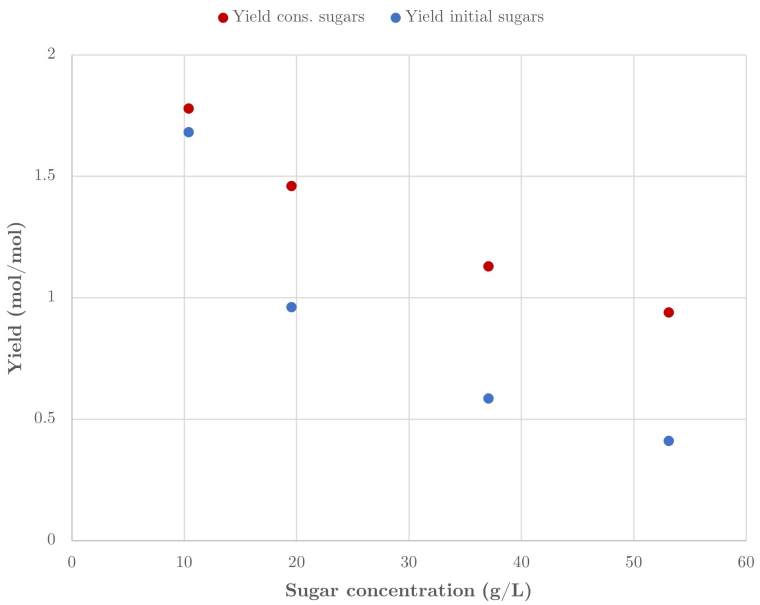

Figure 3.7: Product yields in cultures of *M. thermoacetica* with different sugar concentrations (glucose and xylose at 2:1 mass ratio). **(Red markers)** acetic acid yield on consumed sugars; **(Blue markers)** acetic acid yield on initial sugars.

according to Wang and Wang [47]. This implies that the cessation of growth may be attributed to the presence of undissociated acetic acid and not of acetate.

In line with the previous experiment, yield calculations that consider both consumed and initial sugar concentrations exhibited a decline with rising substrate concentration (Fig. 3.7), and the obtained values were consistently below the theoretical maximum. Regrettably, the concentrations of ethanol and formic acid were not quantified for this test.

A repetition of this substrate inhibition test, using the same concentrations of glucose and xylose in a 2:1 mass ratio, was carried out and the headspace gas composition was alayzed. The percentage of hydrogen, measured upon reaching maximum optical density (Fig. 3.8), increased in cultures with higher sugar concentrations, closer to xylose inhibitory levels. This aligns with the hypothesis proposed by Kellum and Drake [20], suggesting a potential increase in hydrogenase activity in sub-optimal conditions. However, the underlying mechanism for this phenomenon remains uncertain.

Additionally, hydrogen production is commonly associated with the disposal of surplus electrons generated during metabolism [22]. So, the enhanced production of H_2 could

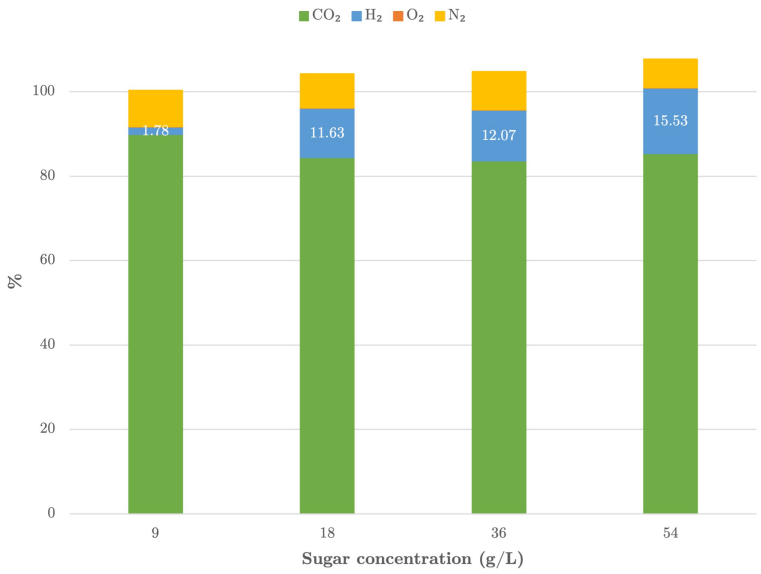

Figure 3.8: Headspace composition of substrate inhibition test with glucose and xylose in a 2:1 mass ratio for *M. thermoacetica* when maximum OD_{600} was reached.

potentially be correlated with the increased availability of reducing power stemming from elevated substrate concentrations.

The specific growth rate was determined during the exponential phase using Equation 3.1. The highest specific growth rate, 0.147 h^{-1}, was observed with a total sugar concentration of 36 g/L. Despite reaching the highest OD_{600}, the bottles containing 54 g/L of sugars exhibited the slowest growth rate at 0.072 h^{-1} (Fig. 3.9).

Given the effective representation of experimental data in the substrate inhibition test with xylose using the Luong model, its applicability in the case of a dual-substrate system involving both xylose and glucose was explored. The dynamic behavior of such a dual-substrate system differs significantly from single-sugar fermentations, and the kinetic equations for the two substrates are expressed as follows [38]:

$$\mu_1 = \frac{\mu_{max,1}\, S_1}{K_{s,1} + S_1}\left(1 - \frac{S_1}{S_{m,1}}\right)^{n_{S,1}} \tag{3.12}$$

$$\mu_2 = \frac{\mu_{max,2}\, S_2}{K_{s,2} + S_2}\left(1 - \frac{S_2}{S_{m,2}}\right)^{n_{S,2}}\left(\frac{1}{1 + K_{CCR}\, S_1}\right) \tag{3.13}$$

$$\mu = \mu_1 + \mu_2 \tag{3.14}$$

Here, μ_i represents the specific growth rate associated with substrate i (i = 1 for xylose and i = 2 for glucose), and K_{CCR} is an inhibitory constant reflecting substrate-induced catabolic repression. If no catabolic repression exists, then K_{CCR} is zero.

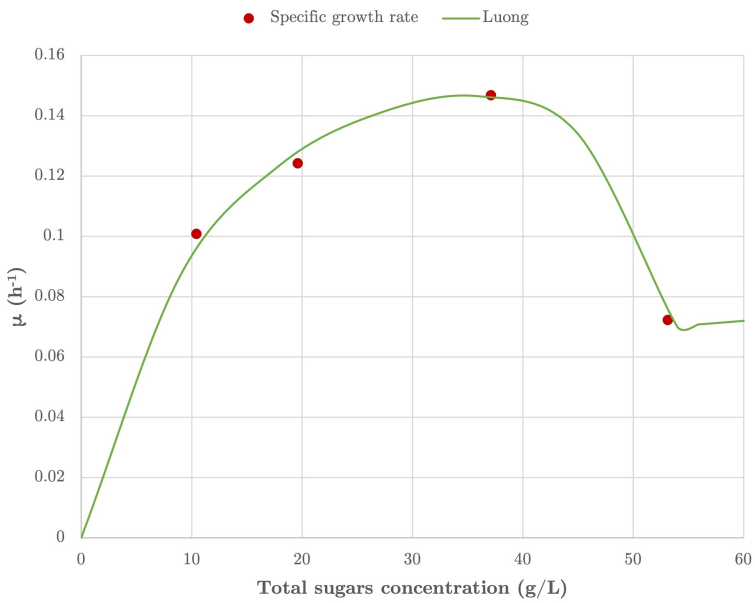

Figure 3.9: Dependence of maximum specific growth rate on substrate concentration according to Luong model for a dual-substrate system for *M. thermoacetica*.

Table 3.3 summarizes the estimated kinetic parameters for *M. thermoacetica* growing on glucose and xylose using the Luong model for a dual-substrate system, calculated by minimizing the MSE. The parameters μ_1, $K_{S,1}$, and $n_{S,1}$ were not directly estimated but were derived from the results of the inhibition test conducted on xylose only.

Considering the dual-substrate system, the maximum xylose concentration ($Sm, 1$) that inhibits growth is markedly lower than in the previous case. This outcome is not surprising, given that, while the phenomenological models aptly describe the batch experiments of cell growth, the parameters are significantly influenced by the varied loading of identical nutrients [26]. Nonetheless, the high coefficient of determination affirms the proficiency of the Luong model in representing inhibitory effects induced by two substrates simultaneously.

The maximum specific growth rate on glucose proves to be inferior to that on xylose; and the inhibitory effect of glucose on *M. thermoacetica* is lower compared to xylose, as evidenced by the higher value of $Sm, 2$ relative to $Sm, 1$. The high value of $Sm, 2$ suggests indeed that this strain is not inhibited by the presence of the hexose sugar unless really high substrate concentrations are employed.

Furthermore, the low value of K_{CCR} reaffirms the insights obtained from Fig. 3.6c - 3.6f, implying the simultaneous utilization of glucose and xylose without a definite impact of catabolite repression.

Finally, while no concentration entirely inhibits growth, the current model recommends

Table 3.3: Estimated kinetic parameters for *M. thermoacetica* using Luong model for a dual-substrate system.

Parameters		
R^2	0.99	
MSE	$1.25 \cdot 10^{-5}$	
$\mu_{max,1}$	0.15 ± 0.003	h^{-1}
$K_{S,1}$	4.17 ± 0.17	g/L
$S_{m,1}$	15.64 ± 0.14	g/L
$n_{S,1}$	0.16 ± 0.08	
$\mu_{max,2}$	0.10 ± 0.03	h^{-1}
$K_{S,2}$	15.90 ± 0.81	g/L
$S_{m,2}$	136.10 ± 0.14	g/L
$n_{S,2}$	0.001 ± 0.001	
K_{CCR}	0.002 ± 0.001	

operating with a glucose and xylose concentration in a 2:1 mass ratio ranging from 30 to 40 g/L to achieve the highest specific growth rates.

3.3 Batch fermentation

3.3.1 Batch fermentation on xylose

A batch fermentation using *Moorella thermoacetica* on DSM 60 medium, containing xylose (18 g/L) was conducted. Throughout the experiment OD_{600}, pH and redox potential were measured to have an immediate indication on the cell growth level. The obtained results are reported in Table 3.4.

The optical density increased up to a maximum of 2.87, which was reached after approximately 44 hours. The redox potential decreased from -307 mV to -431 mV in the first 20 hours, when growth was most prominent, and then remained approximately constant. A similar trend was observed by Schwartzt and Keller [40]: the redox potential, was decreased as the cells of *Moorella thermoacetica* grew from -350 to -435 mV and then remained between -380 and -415 mV. So, it appears that the cells themselves have the ability to reduce the redox potential.

The concentration of xylose decreased from 16.3 to 5.2 g/L (68%). Acetic acid reached

Table 3.4: Batch fermentation of *Moorella thermoacetica* on DSM 60 medium containing xylose (18 g/L).

Time (h)	OD_{600}	pH	Xylose (g/L)	Acetic Acid (g/L)
0	0.24	6.75	16.27	0.10
20	1.55	6.75	13.21	1.66
23	2.12	6.75	11.92	2.31
26	2.31	6.75	11.35	2.51
29	2.61	6.75	10.27	3.10
44	2.87	6.75	7.09	3.77
70	2.30	6.75	5.24	4.07

a final concentration of 4.07 g/L. Considering the sugar and acetic acid concentrations, the following product yields were calculated:

$$Y_{P/S} = \frac{acetic\,acid\,produced}{xylose\,consumed} = 0.36\,\frac{g}{g} = 0.90\,\frac{mol}{mol} \tag{3.15}$$

$$Y_{P/S} = \frac{acetic\,acid\,produced}{initial\,xylose} = 0.24\,\frac{g}{g} = 0.61\,\frac{mol}{mol} \tag{3.16}$$

The calculated yields are much lower than the theoretical maximum of 2.5 mol/mol associated with growth on xylose and to what has been published in literature. Balasubramanian et al. [2] measured 0.76 g of acetic acid per g of xylose consumed (1.9 mol/mol), starting from 20 g/L of xylose in a medium containing 5 g/L of $NaHCO_3$, and supplemented continuously with CO_2 in the reactor's headspace. Similarly, Schmitt et al. [38] achieved a yield of 0.70 g of total product formed per g of sugar consumed, utilizing 16 g/L of $NaHCO_3$ and continuously sparging filtered and deoxygenated CO_2 at a flow rate of 0.5 L/min into the vessel's bottom.

The lower performance observed in this fermentation may be attributed to the absence of exogenous CO_2. Rosenbaum and Müller [36] proposed that a high bicarbonate concentration in the growth medium is essential for *M. thermoacetica* to facilitate energetically the reduction of CO_2 to formate. This reduction process, coupled with NADPH, is energetically unfavorable, as evidenced by standard oxidation-reduction potentials of -320 mV and -420 mV for $NADP^+$/NADPH and $CO_2/HCOO^-$, respectively [48]. Hence, the absence of sodium bicarbonate and continuous CO_2 flushing may have limited the availability of carbon dioxide for the WLP.

Moreover, Huang et al. [16] observed hydrogen production from *M. thermoacetica* under

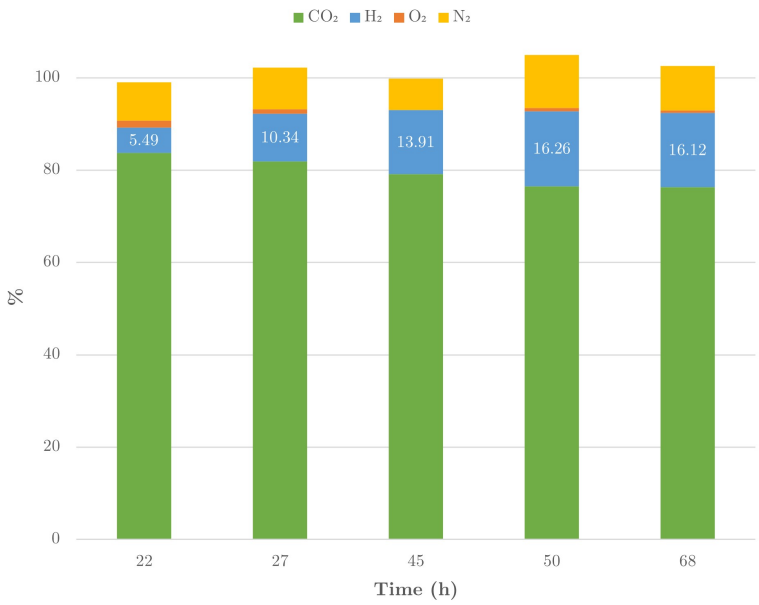

Figure 3.10: Headspace composition of batch fermentation for *M. thermoacetica* on xylose.

conditions of low CO_2, consistent with the increase in H_2% observed in this fermentation (Fig. 3.10). If carbon dioxide is not utilized for the WLP, hydrogen production might be necessary to re-oxidize NADH generated through substrate oxidation and to maintain intracellular redox balance [22]. The excess reducing power is also evidenced by a final ethanol concentration of 1.40 g/L, the production of which requires NADH (Eq. 3.7).

Therefore, the exponential growth phase ended while xylose and ammonium-N were still present, and the pH value was not inhibiting since it was controlled through the addition of NaOH 5 M. The acetate concentration, derived from the total acetic acid concentration using the Henderson-Hasselbalch equation, was calculated to be 0.06 M, lower than the threshold for complete growth inhibition. Growth arrest may have occurred due to the accumulation of an intermediate, such as xylulose, as discussed in Section 3.2. Alternatively, growth inhibition could be due to high levels of intracellular NADH, as observed by Kobayashi et al. [22] using an engineered strain of *M. thermoacetica*.

In order to write the mass balances for a batch fermentation, some assumptions were made. The medium was considered well mixed and homogeneous due to the small volume used in the experiment; temperature and pH were held constant during the fermentation; and product formation was assumed to be only growth-associated, as shown experimentally. Finally, the cell maintenance term, m, was neglected [38].

So, for this isothermal batch reactor with a constant working volume the mass balances are reduced to:

$$\frac{dX}{dt} = r_X \tag{3.17}$$

$$\frac{dS}{dt} = -r_S \tag{3.18}$$

$$\frac{dP}{dt} = r_P \tag{3.19}$$

where X, S, and P, are the biomass, substrate and product concentration, respectively; (r_X), (r_S), and (r_P) are the kinetic rates of microorganism growth, substrate consumption and product formation. The kinetic equations needed to solve the mass balances have to be modified to include both substrate and product inhibition characteristics [24, 38]:

$$r_X = (\mu - K_d)X \tag{3.20}$$

$$\mu = \frac{\mu_{max}\, S}{K_S + S}\Big(1 - \frac{S}{S_m}\Big)^{n_S}\Big(1 - \frac{P}{P_m}\Big)^{n_P} \tag{3.21}$$

$$r_S = \Big(\frac{\mu}{Y_{X/S}}\Big)X \tag{3.22}$$

$$r_P = (\mu\, Y_{P/X})X \tag{3.23}$$

where μ is the specific growth rate of the biomass; K_d is the rate of cell death (considered constant); μ_{max} is the maximum growth rate of cells; K_S is the substrate saturation constant; P_m is the maximum acetic acid concentration; S_m is the maximum substrate concentration; $Y_{X/S}$ and $Y_{P/X}$ are the cell yield and product yield constants, respectively.

The growth rate expression outlined in Eq. 3.21 encompasses several key components. First and foremost, a Monod growth component featuring saturation kinetics is incorporated, wherein growth is constrained by low substrate concentrations. Additionally, an end-product inhibition term is introduced, demonstrating the reduction in growth as the product concentration increases, as evidenced in the product inhibition test. The model used to represent product inhibition was provided by Eq. 3.4, since it gave the best results fitting the experimental data. Moreover, a substrate inhibition term is integrated. The Luong model was used to represent substrate inhibition because, once again, it provided the best fit in the previously described test.

In order to determine the unknown parameters, the differential equations were solved using Euler's first method in an Excel work spreadsheet and the MSE was minimized

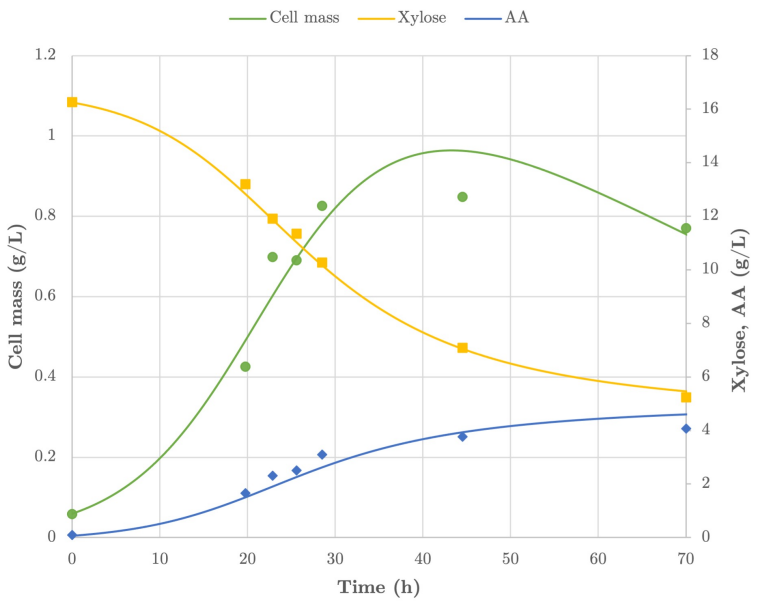

Figure 3.11: Comparison of model prediction (solid lines) and experimental data (markers) for batch fermentation of *M. thermoacetica* on 18 g/L of xylose.

between the empirical and calculated values, represented by markers and solid lines, respectively, in Fig. 3.11. The values of K_S, S_m, and n_S were derived from the substrate inhibition test on xylose only, while K_d was derived from Schmitt et al. [38]. Subsequently, the optimized parameters were μ_{max}, $Y_{X/S}$, $Y_{P/X}$, P_m, and n_P. The respective values are documented in Table 3.4.

The model effectively represents the experimental data, as evidenced by a high coefficient of determination. The estimated μ_{max} appears slightly higher than the one measured during the xylose inhibition test. However, a notable disparity arises in the maximum product concentration, which notably falls below the value observed in dedicated tests (56 g/L). It is important to acknowledge that the model does not incorporate potential constraints beyond substrate or product inhibition that might hinder growth or lead to the accumulation of intermediate products. Therefore, the seemingly low value of P_m minimizing the MSE is attributed to its accounting for growth arrest.

Schmitt et al. [38] reported similar outcomes in their experiment, with the exception of the previously mentioned P_m and of the yields. This discrepancy could be related to the fact that, in their study, they achieved complete xylose consumption and a yield of 0.7, and their model parameters accurately reflect their experimental findings.

Table 3.5: Parameters estimation for batch fermentation of *Moorella thermoacetica* on DSM 60 medium containing xylose (18 g/L).

Parameters	Current estimation	Schmitt et al. (2016)	
R^2	0.96		
MSE	0.06		
μ_{max}	0.22 ± 0.06	0.15 ± 0.20	h^{-1}
K_S	4.17 ± 0.17	2.30 ± 1.34	g/L
S_m	33.98 ± 2.57	-	g/L
n_S	0.16 ± 0.08	-	
$Y_{X/S}$	0.15 ± 0.01	1.53 ± 0.15	g/g
$Y_{P/X}$	2.77 ± 0.21	0.45 ± 0.04	g/g
K_d	0.02 ± 0.01	0.02 ± 0.01	h^{-1}
P_m	5.23 ± 0.87	48	g/L
n_P	1.41 ± 0.43	-	

3.3.2 Batch fermentation on glucose and xylose

A batch fermentation using *Moorella thermoacetica* on DSM 60 medium, containing a combination of glucose (12 g/L) and xylose (6 g/L), was conducted. Throughout the experiment OD_{600} and pH were measured to have an immediate indication on the cell growth level (Table 3.6). The concentration of xylose, glucose, and acetic acid were determined analytically at the end of the fermentation. A lag phase of approximately 20 hours was followed by an exponential phase which lasted until 45 hours after inoculation. The maximum value of OD_{600} was 3.50, which was followed by a stationary phase for almost 20 hours.

After 63 hours, 93% and 16% of the initial xylose and glucose were consumed respectively. The concentration of acetate at pH=6.35 after 63 hours was calculated from the total concentration of acetic acid using the Henderson-Hasselbalch equation. The results obtained were $[CH3COO^-]$ = 0.07 M, not high enough to explain growth inhibition, and [CH3COOH]=0.002 M, much lower than the inhibiting concentration.

Considering both the consumed and initial sugar concentrations, the obtained yields

Table 3.6: Batch fermentation of *Moorella thermoacetica* on DSM 60 medium containing glucose (12 g/L) and xylose (6 g/L).

Time (h)	OD_{600}	pH	Xylose (g/L)	Glucose (g/L)	Acetic Acid (g/L)
0	0.47	6.69	5.45	10.87	0.15
14	0.60	6.68	4.91	10.63	0.37
17	0.70	6.67	4.73	10.59	0.46
20	0.80	6.65	4.34	10.04	0.58
22	0.94	6.52	4.17	10.15	0.77
39	2.87	6.35	2.07	10.03	2.83
41	3.28	6.35	1.61	9.70	3.22
45	3.48	6.35	1.23	9.30	3.55
47	3.50	6.35	1.02	9.35	3.77
63	3.69	6.35	0.39	9.16	4.45

were calculated.

$$Y_{P/S} = \frac{acetic\,acid\,produced}{sugars\,consumed} = 0.63\,\frac{g}{g} = 1.66\,\frac{mol}{mol} \tag{3.24}$$

$$Y_{P/S} = \frac{acetic\,acid\,produced}{initial\,sugars} = 0.26\,\frac{g}{g} = 0.74\,\frac{mol}{mol} \tag{3.25}$$

The results obtained in this study are notably lower than those reported in the literature. In their work, Ehsanipour et al. [12] achieved a yield of 0.771 g of produced acid per g of total initial sugars, starting with a glucose concentration of 19.4 g/L and a xylose concentration of 9.5 g/L. Their experimental setup included a medium with 16 g/L of $NaHCO_3$ and a CO_2 gas flow rate of 1 standard liter per minute (SLPM).

Given that carbon constitutes 40% of both glucose and xylose molecules, the total carbon content derived from the consumed substrate was calculated to be 3.84 g/L. Of this, 1.90 g/L was identified in the produced acetic acid, while, considering the typical chemical formula of dry bacterial biomass as $CH_{2.08}O_{0.53}N_{0.24}$ [14], 0.56 g/L was estimated to have been converted into biomass. The use of the remaining 1.38 g/L of carbon remains uncertain. It is possible that the two molecules of CO_2 generated during glycolysis were not assimilated into acetate via the WLP, explaining the lower yield compared to the theoretical maximum. Should the WLP not have proceeded, NADH might have been regenerated, consequently producing hydrogen. The analysis of the headspace composition indicated, in fact, a progressive increase in the percentage of H_2 over time.

The acetate concentration was found not to be inhibitory, and pH control was maintained through the addition of NaOH 5 M. Possible explanations for this growth arrest include the accumulation of an intermediate product, such as xylulose, or growth inhibition due to an excess of reducing agent.

Using the same assumptions made for the previous fermentation, the mass balances of the isothermal batch reactor can be written as:

$$\frac{dX}{dt} = r_X \tag{3.26}$$

$$\frac{dS_1}{dt} = -r_{S_1} \tag{3.27}$$

$$\frac{dS_2}{dt} = -r_{S_2} \tag{3.28}$$

$$\frac{dP}{dt} = r_P \tag{3.29}$$

where X, S_i (i=1 for xylose, i=2 for glucose), and P, are the biomass, substrates and product concentration, respectively; (r_X), (r_{S_i}), and (r_P) are the kinetic rates of microorganism growth, substrates consumption and product formation. And the kinetic equations are modified as follow, to represent the dual-substrate system:

$$r_X = ((\mu_1 + \mu_2) - K_d)X \tag{3.30}$$

$$\mu_1 = \frac{\mu_{max,1}\, S_1}{K_{S_1} + S_1}\Big(1 - \frac{S_1}{S_{m,1}}\Big)^{n_{S,1}}\Big(1 - \frac{P}{P_m}\Big)^{n_P} \tag{3.31}$$

$$\mu_2 = \frac{\mu_{max,2}\, S_2}{K_{S_2} + S_2}\Big(1 - \frac{S_2}{S_{m,2}}\Big)^{n_{S,2}}\Big(1 - \frac{P}{P_m}\Big)^{n_P}\Big(\frac{1}{1 + K_{CCR}\, S_1}\Big) \tag{3.32}$$

$$r_{S_1} = \Big(\frac{\mu_1}{Y_{X/S,1}}\Big)X \tag{3.33}$$

$$r_{S_2} = \Big(\frac{\mu_2}{Y_{X/S,2}}\Big)X \tag{3.34}$$

$$r_P = (\mu_1\, Y_{P/X,1} + \mu_2\, Y_{P/X,2})X \tag{3.35}$$

where μ_i is the specific growth rate of the biomass on component i; K_d is the rate of cell death (considered constant); $\mu_{max,i}$ is the maximum growth rate of cells on i; $K_{S,i}$ is the substrate saturation constant; P_m is the maximum acetic acid concentration; $S_{m,i}$ is the maximum concentration of substrate i; $Y_{X/S,i}$ and $Y_{P/X,i}$ are the cell yield and product yield constants, respectively. The additional term in Eq. 3.32 is related to the CCR.

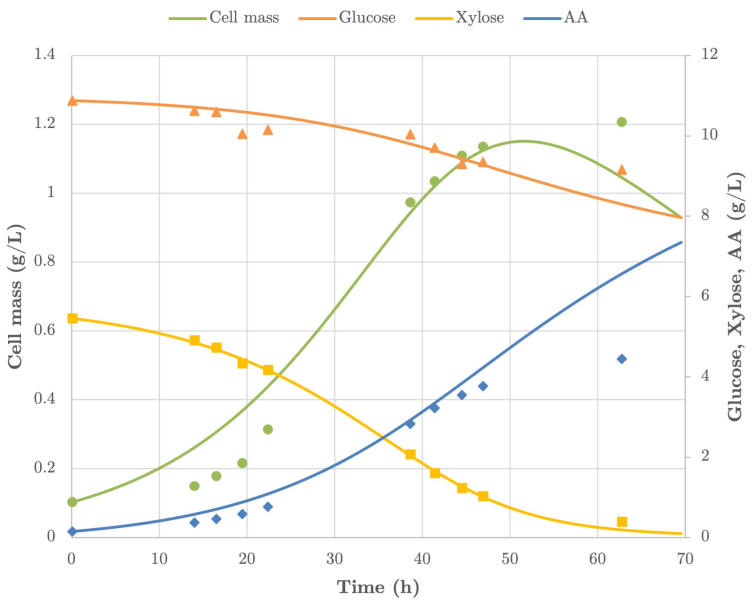

Figure 3.12: Comparison of model prediction (solid lines) and experimental data (markers) for batch fermentation of *M. thermoacetica* on 12 g/L of glucose and 6 g/L of xylose.

In order to determine the unknown parameters, the differential equations were solved using Euler's first method in an Excel work spreadsheet and the MSE was minimized between the empirical and calculated values, represented by markers and solid lines, respectively, in Fig. 3.12. The values of $\mu_{max,1}$, $K_{S,1}$, $S_{m,1}$, $n_{S,1}$, $\mu_{max,2}$, $K_{S,2}$, $S_{m,2}$, $n_{S,2}$, and K_{CCR} were derived from the substrate inhibition test on glucose and xylose. Following this, the optimized parameters were $Y_{X/S1}$, $Y_{P/X1}$, $Y_{X/S2}$, $Y_{P/X2}$, P_m, n_P, and K_d. The respective values are documented in Table 3.7.

The model represents well all the experimental data except for the final sample, where it over-estimates both acetic acid production and glucose consumption. This is also highlighted by a lower coefficient of determination compared the previous fermentation. Once again, a disparity arises in the maximum product concentration, which falls below the value observed in dedicated tests (56 g/L), and is accompanied by a considerable degree of uncertainty. This discrepancy may likely be attributed to P_m accounting for growth arrest, as the model does not account for other factors.

Schmitt et al. [38] obtained similar values for $\mu_{max,1}$, $K_{S,1}$, $K_{S,2}$, and K_d. However, notable disparities emerged in the maximum specific growth rate of *M. thermoacetica* on glucose and in the value of K_{CCR}. This discrepancy is understandable, as they observed an accelerated growth rate upon xylose depletion, whereas in the present experiment, growth

Table 3.7: Parameters estimation for batch fermentation of *Moorella thermoacetica* on DSM 60 medium containing glucose (12 g/L) and xylose (6 g/L).

Parameters	Current estimation	Schmitt et al. (2016)	
R^2	0.94		
MSE	0.03		
$\mu_{max,1}$	0.15 ± 0.003	0.08	h^{-1}
$K_{S,1}$	4.17 ± 0.17	1.23	g/L
$S_{m,1}$	15.64 ± 0.14	-	g/L
$n_{S,1}$	0.16 ± 0.08	-	
$Y_{X/S,1}$	0.30 ± 0.06	1.12	g/g
$Y_{P/X,1}$	0.26 ± 0.43	0.45	g/g
$\mu_{max,2}$	0.10 ± 0.03	0.44	h^{-1}
$K_{S,2}$	15.90 ± 0.81	10.8	g/L
$S_{m,2}$	136.10 ± 0.14	-	g/L
$n_{S,2}$	0.001 ± 0.001	-	
$Y_{X/S,2}$	0.58 ± 0.19	1.71	g/g
$Y_{P/X,2}$	4.02 ± 0.67	0.49	g/g
K_d	0.05 ± 0.02	0.03	h^{-1}
P_m	10.83 ± 60.03	48	g/L
n_P	0.16 ± 1.00	-	
K_{CCR}	0.002 ± 0.001	1.37	g/L

ceased upon the exhaustion of the pentose sugar. Furthermore, the absence of a definite glucose uptake throughout the whole fermentation process complicates the attribution of this behavior to carbon catabolite repression (CCR).

The yield values also differ, with the current model indicating low cell yield constants. This discrepancy reflects the relatively low amount of cell mass obtained, maximizing at 1.20 g/L. In contrast, Schmitt et al. [38] achieved 16 g/L of biomass and complete sugar consumption (10 g/L glucose and 10 g/L xylose).

Chapter 4

Acetic acid production by *T. kivui*

4.1 Product inhibition test

The impact of increasing acetate concentrations was assessed for *Thermoanaerobacter kivui* cultures growing on 18 g/L of glucose. The product inhibition closely mirrors the patterns observed in *Moorella thermoacetica*, shedding light on the robustness of these microbial responses to sodium acetate. Across the various cultures containing sodium acetate, the OD_{600} values exhibited a consistent decrease with increasing concentrations of sodium acetate. Moreover, temporal shifts were observed, resulting in extended durations, as illustrated in Figure 4.1a.

In particular, cultures with initial acetate concentrations of 0.58 and 0.68 M, exhibited

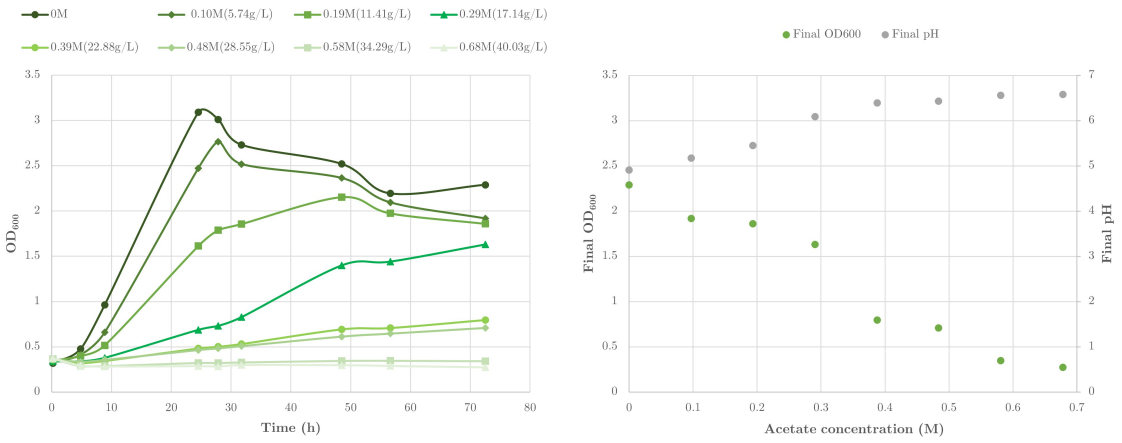

(a) **(b)**

Figure 4.1: Effect of initial increasing acetate concentrations **(a)** on OD_{600} and **(b)** on final OD_{600} and pH for *T. kivui*.

Table 4.1: Models used for prediction of product inhibition and their estimated parameters for *T. kivui*.

Model	**Equation**	**Parameters**	**MSE**	$\mathbf{R^2}$
Ghose-Tyagi	$\mu = \mu_0\left(1 - \frac{P}{P_m}\right)$	$\mu_0 = 0.09\ \mathrm{h}^{-1}$ $\mathrm{P}_m = 0.61\ \mathrm{M}$	$8.47 \cdot 10^{-5}$	0.93
Eq. 3.3	$\mu = \mu_0\left(1 - \left(\frac{P}{P_m}\right)^{n_P}\right)$	$\mu_0 = 0.10\ \mathrm{h}^{-1}$ $\mathrm{P}_m = 0.62\ \mathrm{M}$ $\mathrm{n}_P = 0.82$	$7.25 \cdot 10^{-5}$	0.94
Eq. 3.4	$\mu = \mu_0\left(1 - \frac{P}{P_m}\right)^{n_P}$	$\mu_0 = 0.10 \pm 0.02\ \mathrm{h}^{-1}$ $\mathrm{P}_m = 0.58 \pm 0.08\ \mathrm{M}$ $\mathrm{n}_P = 1.03 \pm 0.40$	$5.22 \cdot 10^{-5}$	0.95

negligible growth, indicating a critical limit for microbial proliferation.The final pH values (Fig. 4.1b) exhibited a downward trend corresponding to decreasing initial sodium acetate concentrations. This phenomenon was attributed to the heightened production of acetic acid as a metabolic product.

When the acetate concentration reached 0.68 M (equivalent to 34.3 g/L), the specific growth rate (Eq. 3.1) dropped to 0 h^{-1}. This abrupt decline in μ with respect to the product concentration underscores the importance of product inhibition in influencing the microbial dynamics. The decline in μ with respect to P can still be aptly described using Eqs. 3.2 - 3.4. Figure 4.2 and Table 4.1 illustrate how the before-mentioned models align with experimental data, revealing greater consistency among the results obtained by applying the MSE method to the three different equations.

It's noteworthy that the utilization of an equation with two parameters, as opposed to the Ghose-Tyagi model, yielded a marginal enhancement in the fit.

The optimal value of P_m, which minimizes the MSE, aligns with the findings of the serum vial test. In a study by Klemps et al. [21], a higher limit for *Thermoanaerobacter kivui* was reported, indicating complete bacterial growth inhibition when the acetate concentration reached 0.8 M. In contrast, von Eysmondt et al. [13] observed, through continuous fermentation, that the maximum acetate concentration supporting positive growth and dilution rates was 0.575 M. This value is closer to the one determined by the proposed models.

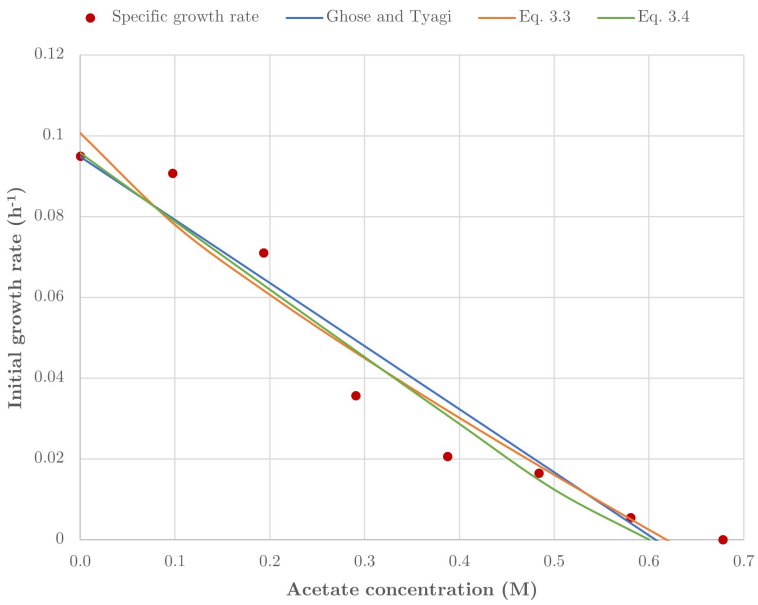

Figure 4.2: Dependence of maximum specific growth rate on acetate concentration according to Eq. 3.2-3.4 for *T. kivui*.

4.2 Substrate inhibition test

The substrate inhibition test was replicated to assess the influence of increasing glucose concentrations on the specific growth rates of *Thermoanaerobacter kivui*.

Throughout the experiment, OD_{600} and pH were consistently measured, and the trends, averaged from duplicate results, are depicted in Fig. 4.3a and 4.3b. None of the sugar concentrations induced complete growth inhibition. In contrast to *M. thermoacetica*, there was no growth delay even at the highest concentrations. According to von Eysmondt et al. [13], substrate inhibition from glucose on this strain is considerably smaller than the corresponding product inhibition.

For all the conditions pH dropped to values close to 5, which could have inhibited growth, which did not seem to be particularly affected even after the addition of extra 2 mL of NaOH 1 M after 25 hours.

Once again, the final concentration of acetic acid obtained in the different conditions did not reflect the great difference in the initial substrate concentrations (Fig. 4.3c - 4.3f), except for the cultures containing 9 g/L of glucose, which was completely consumed after 24 hours. For the other conditions, the concentration of acetic acid went from a minimum of 11.86 g/L for the culture growing on 18 g/L of glucose to a maximum of 12.43 g/L for the culture with 54 g/L of glucose. The concentrations of undissociated acetic acid were

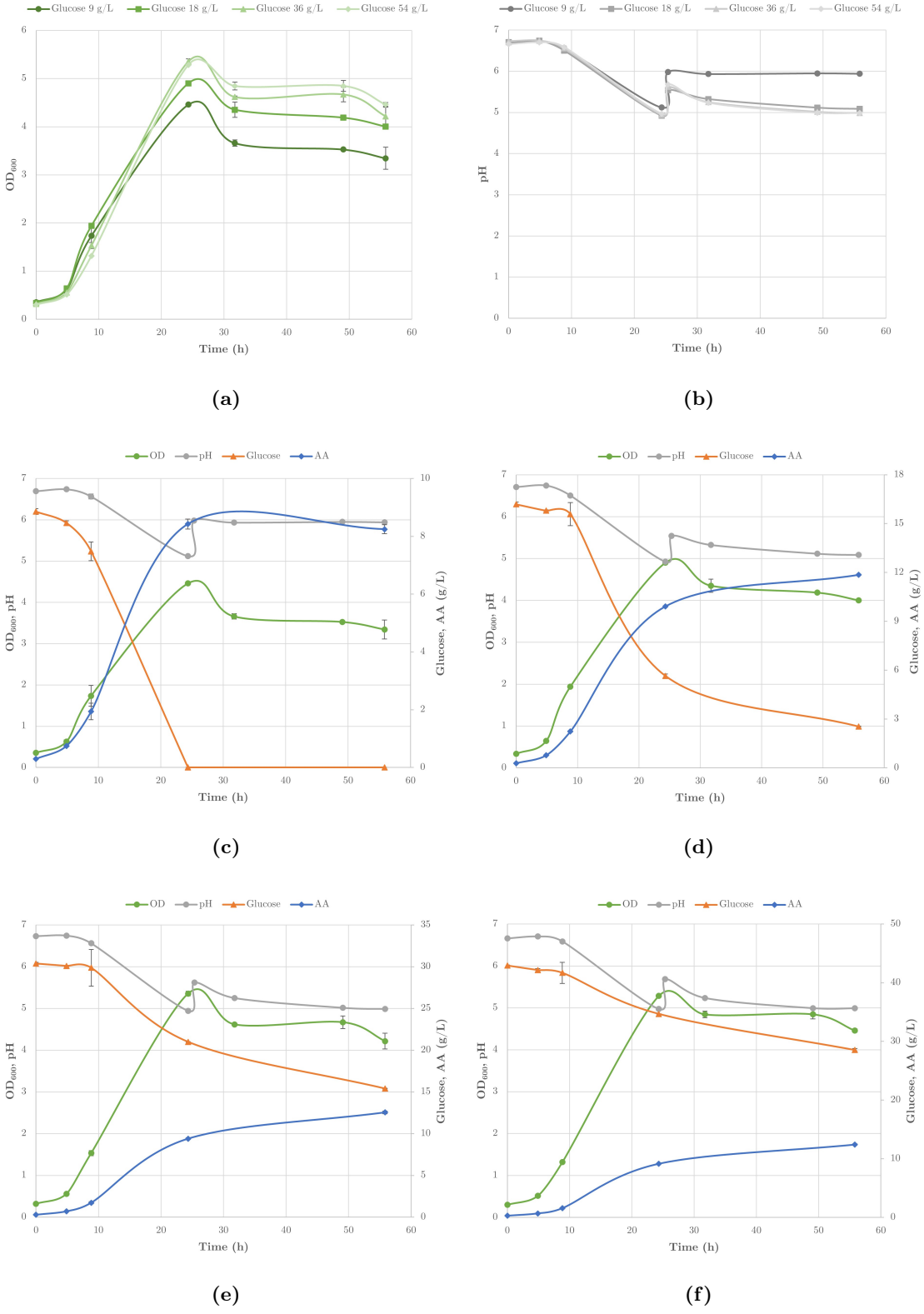

Figure 4.3: Evolution of **(a)** OD_{600}, **(b)** pH, glucose, and acetic acid in cultures of *T. kivui* at increasing glucose concentrations: **(c)** 9 g/L, **(d)** 18 g/L, **(e)** 36 g/L, and **(f)** 54 g/L.

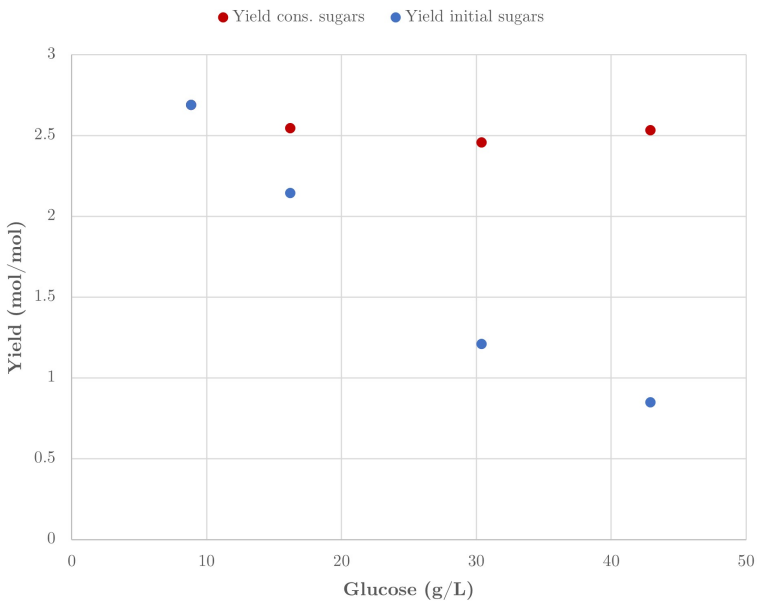

Figure 4.4: Product yields in cultures of *T. kivui* with different glucose concentrations. **(Red markers)** acetic acid yield on consumed glucose; **(Blue markers)** acetic acid yield on initial glucose.

determined to be 0.01 M, 0.07 M, 0.08 M, and 0.08 M for cultures containing 9 g/L, 18 g/L, 36 g/L, 54 g/L of glucose respectively. If the inhibition of *T. kivui* by undissociated acid mirrors that of *M. thermoacetica*, the findings imply that product inhibition may be responsible for growth cessation across all concentrations, with the exception of the first one.

Yield calculations, factoring both consumed and initial sugar concentrations (Fig. 4.4), demonstrated the expected decrease in yield with increasing glucose concentration due to the higher fraction of unutilized sugar. Unlike *M. thermoacetica*, the difference in yield calculated with consumed sugar was less pronounced. The yield, based on the consumed sugars, consistently exceeded 2 mol/mol, indicating the simultaneous activity of both the WLP and glycolysis.

The analysis revealed that ethanol and formic acid were not produced as by-products. The concentration of ethanol was consistently at zero, while formic acid was measured in the first three sample points and then went to zero.

The specific growth rate was calculated during the exponential phase. Unlike *M. thermoacetica*, the specific growth rate increased progressively with the increasing substrate concentrations. The highest growth rate, 0.12 h^{-1}, was obtained using 54 g/L of glucose

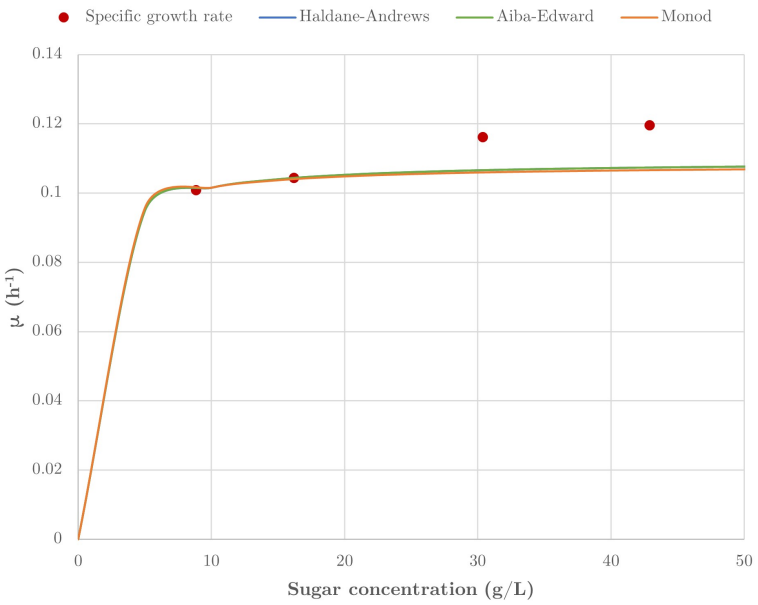

Figure 4.5: Dependence of maximum specific growth rate on substrate concentration according to Haldane-Andrews, Aiba-Edward, and Monod models for *T. kivui*.

while the lowest was measured for 9 g/L of glucose, 0.10 h^{-1}.

The attempts to align the experimental data with both the Haldane-Andrews model (Eq. 3.9) and the Aiba-Edward model (Eq. 3.10) yielded more favorable outcomes compared to the analogous attempts with *M. thermoacetica* (Fig. 4.5). These models exhibited effective alignment with the initial two sample points; however, their predictive accuracy diminished for the subsequent two points at higher concentrations. Upon employing the Solver add-in function in Microsoft Excel for model parameter determination, minimizing the MSE between the experimental and calculated values, the Haldane-Andrews model and the Aiba-Edward models yielded the values presented in Table 4.2.

The high value of the parameter K_i may appear unreasonable. However, it is crucial to interpret this value as indicative of the degree of inhibition within a specific system. A higher K_i value suggests a less severe inhibition degree [5]. In this context, the elevated K_i value implies that *T. kivui* is apparently unaffected by substrate inhibition.

Given the apparent insensitivity of this strain to substrate inhibition, the Monod model (Eq. 3.8) was employed to fit the experimental data. Remarkably, the obtained values were comparable to those derived from the Haldane-Andrews and Aiba-Edward models (Tab. 4.2).

This convergence across models reinforces the indication that *T. kivui* exhibits minimal susceptibility to substrate inhibition, affirming the robustness of the observed experimental

Table 4.2: Models used for prediction of substrate inhibition and their estimated parameters for *T. kivui*.

Model	Equation	Parameters	MSE	R^2
Haldane-Andrews	$\mu = \mu_{max}\frac{S}{K_S+S+\frac{S^2}{K_i}}$	$\mu_{max} = 0.11\ h^{-1}$ $K_S = 0.77$ g/L $K_i = 3.37 \cdot 10^5$ g/L	$4.61 \cdot 10^{-6}$	0.97
Aiba-Edward	$\mu = \frac{\mu_{max}S}{K_s+S}\exp\left(-\frac{S}{K_i}\right)$	$\mu max = 0.11\ h^{-1}$ $K_S = 0.77$ g/L $K_i = 1.72 \cdot 10^5$ g/L	$4.61 \cdot 10^{-6}$	0.97
Monod	$\mu = \mu_{max}\frac{S}{K_S+S}$	$\mu_{max} = 0.11 \pm 0.01\ h^{-1}$ $K_S = 0.66 \pm 1.98$ g/L	$5.54 \cdot 10^{-6}$	0.97

trends. Furthermore, working with glucose concentrations exceeding 10 g/L seems to guarantee enhanced specific growth rates.

4.3 Batch fermentation

A batch fermentation of *Thermoanaerobacter kivui* was conducted on 36 g/L of glucose. Throughout the experiment OD_{600}, pH and the redox potential were measured to have an immediate indication on the cell growth level (Table 4.3). The concentration of glucose and of acetic acid were determined analytically at the end of the fermentation.

The OD_{600} showed a continuous increase, peaking at 6.13 around the 31-hour mark and maintaining a nearly constant level up to 52 hours. Concurrently, the redox potential experienced a substantial decrease from -332 mV to -526 mV during the initial 22 hours, corresponding to the period of most pronounced growth, and then stabilized thereafter.

After 52 hours, 45.63% of the initial glucose was consumed. Considering both the consumed and initial sugar concentrations, the obtained yields were calculated.

$$Y_{P/S} = \frac{acetic\ acid\ produced}{glucose\ consumed} = 0.85\ \frac{g}{g} = 2.54\ \frac{mol}{mol} \tag{4.1}$$

$$Y_{P/S} = \frac{acetic\ acid\ produced}{initial\ glucose} = 0.39\ \frac{g}{g} = 1.16\ \frac{mol}{mol} \tag{4.2}$$

Since the yield calculated considering the consumed sugars is higher than 2 mol/mol, the Acetyl-CoA pathway must be active together with glycolysis. However, the precise reasons for the yield being lower than 3 mol/mol remain unclear. The ethanol concentration was

Table 4.3: Batch fermentation of *Thermoanaerobacter kivui* on DSM 60 medium containing glucose (36 g/L).

Time (h)	OD_{600}	pH	Glucose (g/L)	Acetic Acid (g/L)
0	0.22	6.86	32.06	0.29
5	0.37	6.79	31.42	0.54
22	4.56	6.37	26.47	5.70
27	5.07	6.35	23.18	8.18
31	6.22	6.35	21.47	9.68
46	6.12	6.35	17.35	12.58
52	6.39	6.35	17.43	12.66

below the calibration line for every sample point, while the formic acid concentration increased from 0.022 g/L to 0.035 g/L in the first five hours and then it went to zero. Thus, neither ethanol nor formic acid appear to be contributing to the reduced yield. It is conceivable that a portion of the glucose was utilized for biomass production.

The results obtained, however, are consistent with the results obtained by Klemps et al. [21], who registered a yield of 2.55 mol/mol (85% of the theoretical maximum) of acetic acid per glucose consumed, when starting with 50 g/L of substrate and pH controlled at 6.4.

The concentration of ammonium nitrogen was calculated at the beginning of the fermentation (270 mg/L) and after 46 hours (187 mg/L). So, when the exponential phase stopped, as previously observed for *Moorella thermoacetica*, glucose and ammonium-N were still available. pH was controlled by the addition of NaOH 5 M so it should not have been inhibiting. The acetate concentration at the pH value of the fermentation broth, was calculated from the total acetic acid concentration using the Henderson-Hasselbalch equation and it was 0.20 M (12.10 g/L). This concentration, according to the product inhibition test, was not high enough to result in complete growth inhibition. As a consequence, it is still unclear why cell growth and product formation stopped. It is possible that part of the CO_2 produced during glycolysis was not effectively reconverted into acetate, leading to an accumulation of NADH and subsequent growth inhibition.

A model for the isothermal batch reactor with a constant working volume used for the growth of *T. kivui* on glucose, using the same assumptions used for *M. thermoacetica* (medium well mixed and homogeneous, temperature and pH constant during fermentation,

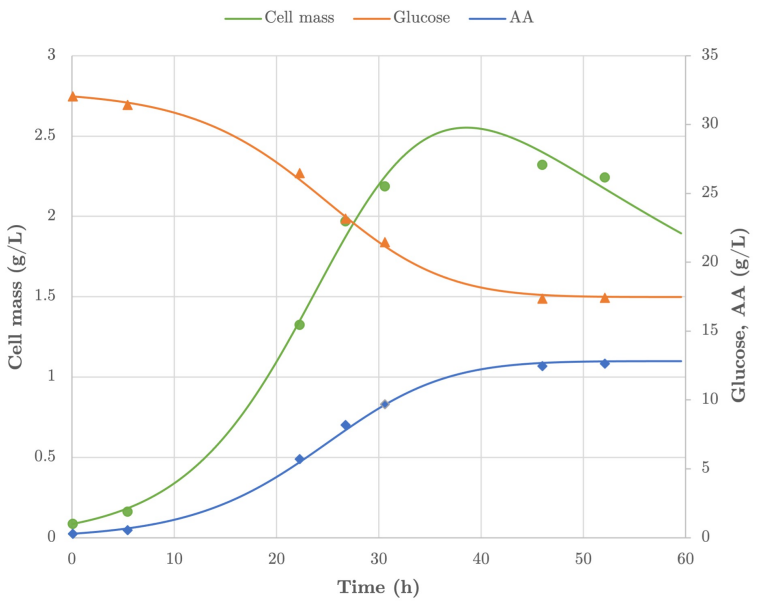

Figure 4.6: Comparison of model prediction (solid lines) and experimental data (markers) for batch fermentation of *T. kivui* on 36 g/L of glucose.

and product formation only growth-associated) can be written as:

$$\frac{dX}{dt} = r_X \tag{4.3}$$

$$\frac{dS}{dt} = -r_S \tag{4.4}$$

$$\frac{dP}{dt} = r_P \tag{4.5}$$

where X, S, and P, are the biomass, glucose and acetic acid concentration, respectively; (r_X), (r_S), and (r_P) are the kinetic rates of microorganism growth, substrate consumption and product formation.

The kinetic equations are modified as follows:

$$r_X = (\mu - K_d)X \tag{4.6}$$

$$\mu = \frac{\mu_{max}\, S}{K_S + S}\left(1 - \frac{P}{P_m}\right)^{n_p} \tag{4.7}$$

$$r_S = \left(\frac{\mu}{Y_{X/S}}\right)X \tag{4.8}$$

$$r_P = (\mu\, Y_{P/X})X \tag{4.9}$$

where μ is the specific growth rate; K_d is the rate of cell death (considered constant); μ_{max} is the maximum growth rate of cells; K_S is the substrate saturation constant; P_m is the

Table 4.4: Parameters estimation for batch fermentation of *Thermoanaerobacter kivui* on DSM 60 medium containing glucose (36 g/L).

Parameters		
R^2	0.99	
MSE	0.03	
μ_{max}	0.17 ± 0.008	h^{-1}
K_S	0.66 ± 1.98	g/L
$Y_{X/S}$	0.24 ± 0.07	g/g
$Y_{P/X}$	3.53 ± 0.005	g/g
K_d	0.02 ± 0.03	h^{-1}
P_m	12.81 ± 0.49	g/L
n_P	0.78 ± 2.38	

maximum acetic acid concentration inhibiting growth; $Y_{X/S}$ and $Y_{P/S}$ are the cell yield and product yield constants, respectively.

Equation 4.7 is formulated in this manner based on the outcomes of the product inhibition test conducted with *Thermoanaerobacter kivui*. The results of this test demonstrated that Equation 3.4 provides the most accurate representation of product inhibition for this particular strain.

Furthermore, the substrate inhibition test indicated that high substrate concentrations do not significantly impact *T. kivui*, confirming that the Monod model can accurately describe microbial growth for this strain. These equations were integrated using Euler's method and the parameters were estimated minimizing the MSE between the empirical and calculated values, represented by markers and solid lines, respectively, in Fig. 4.6.

The value for $K_{S,1}$ was derived from the substrate inhibition test on glucose. Thus, the optimized parameters were μ_{max}, $Y_{X/S}$, $Y_{P/X}$, K_d, P_m, and n_P. The respective values are documented in Table 4.4.

To the best of my knowledge, no previous kinetic analysis have been conducted for batch fermentations involving *Thermoanaerobacter kivui*. However, in their investigation, Klemps et al. [21], observed a peak specific growth rate of 0.17 h^{-1} during batch fermentations, a result that aligns with the prediction of the current model. However, the optimal P_m value identified to minimize the MSE differs significantly from the one obtained in the product inhibition test, the latter being notably higher (34.8 g/L), probably because, as mentioned

before, P_m accounts for growth arrest in this model. On the other hand, the exponent n_P exhibits greater consistency between the two sets of results.

Chapter 5

Co-culture of *M. thermoacetica* and *T. kivui*

The traditional method used in biotechnologies today centers on the use of monocultures. The main reasons for this preference are that they are easier to monitor, their metabolic pathways are thoroughly understood, and they abide by strict biosafety laws. But monocultures' greatest weakness is that they are easily contaminated, which can result in significant financial losses and waste of feedstock while the culture is in operation.

A promising solution to these problems are co-cultures. These dynamic partnerships between various microbial strains have demonstrated resilience and adaptation in the face of environmental changes, thereby avoiding contamination problems. Even though anaerobic and thermophilic cultures have a lower chance of contamination, co-cultures are still a tempting alternative because of how well they use complicated substrates. By utilizing the combined metabolic activities of the collaborating microbial strains, this technique shows a significant improvement in biomass yields and the synthesis of high-value goods [37].

5.1 Co-culture in serum vials

As *Thermoanaerobacter kivui* demonstrates superior glucose consumption capabilities and *Moorella thermoacetica* exhibits the distinct trait of consuming xylose, the potential for a co-culture arrangement becomes interesting.

To assess the feasibility of a co-culture, a serum vial test was conducted, with optical density and pH serving as metrics for monitoring cell growth and acetic acid production throughout the experiment (Fig. 5.1). Sugar and acetic acid concentrations were measured

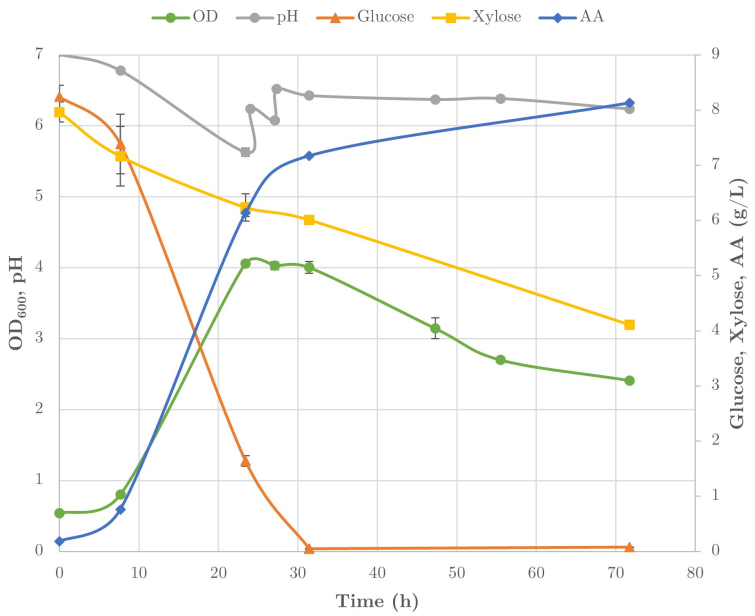

Figure 5.1: Co-culture in serum vials.

after. The test was conducted in duplicate. After 23 hours, the optical density peaked at a maximum value of 4, maintaining stability for approximately 7 hours before experiencing a subsequent decline. By the end of the experiment, the pH had settled near 6.2, a level expected to have no inhibitory effect on either *M. thermoacetica* or *T. kivui*.

Complete glucose consumption was observed after 30 hours, aligning with the phase of most pronounced growth. This rapid glucose consumption coincided with the peak of acetic acid production. On the other hand, only 48% of xylose was consumed. Interestingly, this consumption persisted even as the optical density decreased, although at a slower rate of acetic acid production.

The precise ratio of the two strains at the end of the experiment cannot be determined without more precise examinations, such as DNA analyses. Nevertheless, by observing sugar consumption patterns, it can be supposed that the growth of *T. kivui* was more enhanced, as evidenced by the complete glucose utilization. Simultaneously *M. thermoacetica* also experienced growth, as demonstrated by the partial consumption of the pentose sugar, and possibly contributing to a portion of glucose utilization.

Potential biotic interactions within microbial communities include mutualism, commensalism, competition, or amensalism [37]. Mutualistic relationships rely on nutrient exchange, a scenario not applicable to the interaction between *M. thermoaetica* and *T. kivui*. Commensalism, where one microorganism benefits without harm or advantage to the other, is a conceivable scenario. However, it is more likely that the two microorganisms

engage in competition, as they may not compete for the same energy sources (glucose for *T. kivui* and xylose for *M. thermoacetica*), yet share nitrogen and trace elements, adversely affecting both. Amensalism, characterized by one microorganism inhibiting or destroying another without self-impairment, seems improbable given the observed consumption of both carbon sources.

The yield was computed by taking into account both the initial and consumed sugars:

$$Y_{P/S} = \frac{acetic\ acid\ produced}{sugars\ consumed} = 0.66\ \frac{g}{g} = 1.87\ \frac{mol}{mol} \tag{5.1}$$

$$Y_{P/S} = \frac{acetic\ acid\ produced}{initial\ sugars} = 0.49\ \frac{g}{g} = 1.34\ \frac{mol}{mol} \tag{5.2}$$

These values are not extremely high compared to the theoretical maximum. If all the glucose was converted to acetic acid with a yield of 3 mol/mol, and all xylose was converted with a yield of 2.5 mol/mol, the maximum theoretical yield in a medium containing glucose and xylose in a 1:1 mass ratio would be 2.73 mol/mol.

However, low concentrations of by-products were detected. After 72 hours, 0.19 g/L, 0.74 g/L, and 0.20 g/L of ethanol, lactic acid, and propionic acid, respectively, were measured, while formic acid and butyric acid were absent.

Recalculating the yield considering all the products results in a higher yield, approaching the maximum theoretical:

$$Y_{P/S} = \frac{total\ products}{sugars\ consumed} = 0.77\ \frac{g}{g} = 2.06\ \frac{mol}{mol} \tag{5.3}$$

The concentrations of acetate and undissociated acetic acid were calculated using the Henderson-Hasselbalch equation, revealing values of 0.13 M and 0.005 M, respectively. These concentrations were found to be well below inhibitory levels.

In contrast to the serum vial experiments previously conducted, the co-culture exhibited a diminished performance of *T. kivui* (Table 5.1). Although the acetic acid production and glucose consumption remained comparable, the co-culture exhibited a significantly lower maximum yield. However, when comparing the co-culture to the individual performance of *M. thermoacetica*, an enhancement is evident. Specifically, the co-culture displayed a doubled acetic acid production compared to the individual strain cultivated on xylose only, despite a higher xylose consumption. Furthermore, in the substrate inhibition tests involving glucose and xylose, *M. thermoacetica* exhibited slightly lower acetic acid production, reduced glucose consumption, and a lower overall yield.

Table 5.1: Comparison between the performances of *T. kivui* and *M. thermoacetica* individually in serum vials and those of the co-culture.

	Max yield	**Substrate consumption**	**Acetic Acid**
M. thermoacetica on xylose	1.56 mol/mol	6.53 g/L of xylose (76%)	4.07 g/L
M. thermoacetica on glucose and xylose	1.78 mol/mol	3.84 g/L of xylose (100%) 5.96 g/L of glucose (91%)	6.38 g/L
Co-culture	1.87 mol/mol	3.96 g/L of xylose (48%) 8.17 g/L of glucose (99%)	8.13 g/L
T. kivui on glucose	2.69 mol/mol	8.86 g/L of glucose (100%)	8.25 g/L

This is an encouraging indicator because, while numerous homoacetogens typically favor glucose, the distinctive ability of *Moorella thermoacetica* to utilize xylose makes optimizing its performance interesting.

5.2 Co-culture supplemented with DMSO is serum vials

The metabolomic analysis conducted by Kobayashi et al. [22] on a genetically engineered strain of *Moorella thermoacetica* provided insights into the dynamics of H_2 production and intracellular redox balance. Specifically, they observed a correlation between increased levels of intracellular NADH and the production of H_2, indicating the utilization of excess reducing equivalents for redox balancing. This accumulation of reducing agents was attributed to artificial modifications in the bacterial genome, which disrupted normal metabolic pathways.

It was noted that previous tests within this experimental work might have inadvertently led to NADH accumulation due to the absence of exogenous CO_2 supplementation, a common practice in related literature. This deficiency in CO_2 supplementation implied inefficient utilization of CO_2 generated through glycolysis by the bacteria through the WLP.

Kobayashi et al. [22] further elucidated the adverse effects of elevated intracellular NADH levels on bacterial growth. They demonstrated that increased NADH levels directly hindered growth, as evidenced by growth resumption and complete sugar consumption upon the addition of dimethyl sulfoxide (DMSO), a compound known to lower NADH levels.

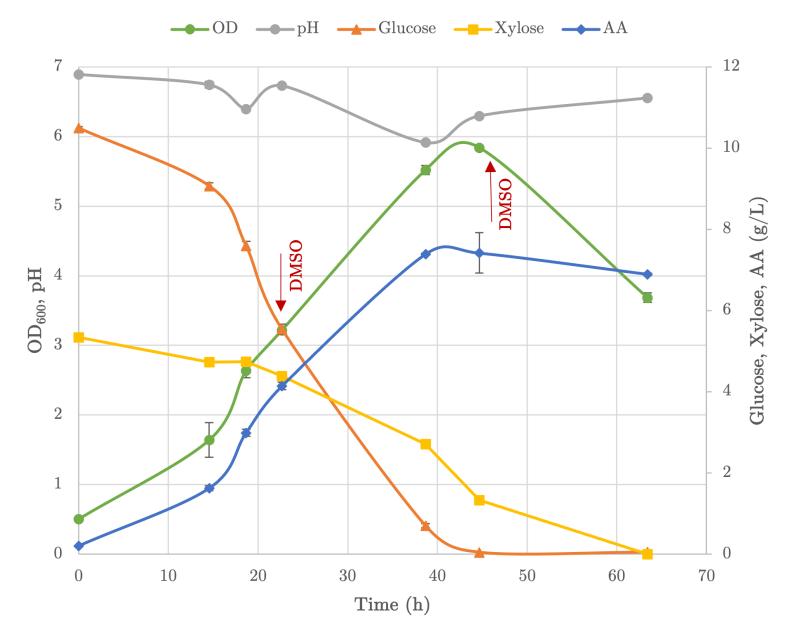

Figure 5.2: Co-culture supplemented with DMSO in serum vials.

To explore the impact of NADH accumulation on growth in prior experiments, a serum vial test was conducted with DMSO added after 24 and 45 hours. Optical density and pH were used for monitoring cell growth and acetic acid production throughout the experiment (Fig. 5.2). Sugar and acetic acid concentrations were measured after the conclusion of the test, which was conducted in duplicate.

The co-culture supplemented with DMSO exhibited enhanced performance, reaching a maximum optical density of 5.84 after 45 hours, higher than without DMSO. Once again, it is not possible to know exactly the ratio between the two bacterial strains. However, this delayed peak suggests heightened growth of *Moorella thermoacetica*. In fact, in the previous serum vials tests conducted, *T. kivui*, usually reached a maximum OD_{600} after approximately 24 hours, and the same was observed in the previous co-culture. On the other hand, *M. thermoacetica* usually reaches the maximum optical density after 40 hours, more in line with the results observed in this test.

By the end of the experiment, the pH had settled near 6.55, through subsequent corrections with NaOH, a level expected to have no inhibitory effect on either *M. thermoacetica* or *T. kivui*. In addition, neither the final concentration of undissociated acetic acid nor acetate should be inhibiting at this pH.

DMSO addition improved co-culture performance, yielding complete sugar consumption, while the final acetic acid concentration was similar to cultures without DMSO. As a

consequence, the overall yield resulted in a lower value compared the previous experiment.

$$Y_{P/S} = \frac{acetic\,acid\,produced}{sugars\,consumed} = \frac{acetic\,acid\,produced}{initial\,sugars} = 0.46\,\frac{g}{g} = 1.28\,\frac{mol}{mol} \tag{5.4}$$

This result was expected, given that DMSO is useful in lowering NADH levels, but it does not stimulate the WLP, essential for maximizing acetic acid production. DMSO is reduced to DMS, and reported cases of bacterial DMSO reduction are NADH-dependent reactions (5.5) [35].

$$DMSO\ +\ 2\,H^{+}\ +\ 2\,e^{-}\ \rightarrow\ DSM\ +\ 2\,H_2O \tag{5.5}$$

Thus, it is evident that additional strategies are required to improve yield. Since growth inhibition due to the halted WLP was observed in this experiment, supplying exogenous CO_2 emerges as a crucial step for optimizing metabolic function and enhancing overall yield.

Using the same assumptions made for the previous fermentations, a kinetic model was applied to the DMSO-supplemented co-culture. This model, utilizing parameters previously determined, aimed to ascertain its ability to represent the observed outcomes. The mass balances can be written as:

$$\frac{dX}{dt} = r_{X_{MT}} + r_{X_{TK}} \tag{5.6}$$

$$\frac{dS_1}{dt} = -r_{S_1} \tag{5.7}$$

$$\frac{dS_2}{dt} = -r_{S_2} \tag{5.8}$$

$$\frac{dP}{dt} = r_P \tag{5.9}$$

where X is the biomass concentration, constituted by the combination of the two microorganisms, denoted as X_{MT} and X_{TK}. For the purposes of this analysis, a 1:1 ratio between the two strains was assumed, established by initially adding an appropriate volume to achieve OD_{600}=0.1 for each strain at t=0. S_i (i=1 for xylose, i=2 for glucose), and P, are the substrates and product concentration, respectively; ($r_{X_{MT}}$), ($r_{X_{TK}}$)(r_{S_i}), and (r_P) are the kinetic rates of the two microorganisms growth, substrates consumption and product formation. For simplicity, the rate of cell death, K_d, and the maintenance term, m, were omitted.

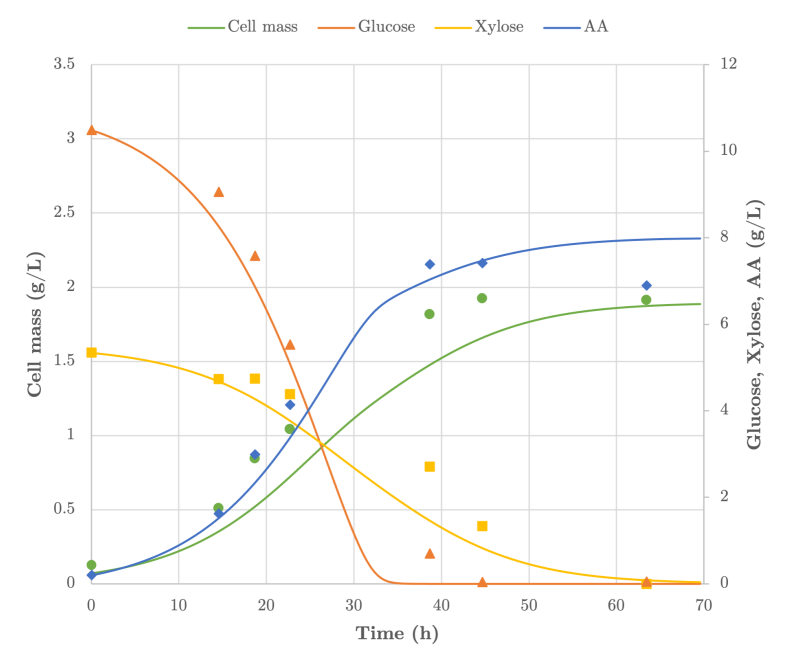

Figure 5.3: Comparison of model prediction (solid lines) and experimental data (markers) for DMSO-supplemented co-culture on 12 g/L of glucose and 6 g/L of xylose.

The kinetic equations are modified as follow, to represent the two bacterial strains:

$$r_{X_{MT}} = (\mu_1 + \mu_2) X_{MT} \tag{5.10}$$

$$\mu_1 = \frac{\mu_{max,1}\, S_1}{K_{S_1} + S_1} \left(1 - \frac{S_1}{S_{m,1}}\right)^{n_{S,1}} \left(1 - \frac{P}{P_{m_{MT}}}\right)^{n_{P_{MT}}} \tag{5.11}$$

$$\mu_2 = \frac{\mu_{max,2}\, S_2}{K_{S_2} + S_2} \left(1 - \frac{S_2}{S_{m,2}}\right)^{n_{S,2}} \left(1 - \frac{P}{P_{m_{MT}}}\right)^{n_{P_{MT}}} \left(\frac{1}{1 + K_{CCR}\, S_1}\right) \tag{5.12}$$

$$r_{X_{TK}} = \mu_3\, X_{TK} \tag{5.13}$$

$$\mu_3 = \frac{\mu_{max,3}\, S_2}{K_{S,3} + S_2} \left(1 - \frac{P}{P_{m_{TK}}}\right)^{n_{pTK}} \tag{5.14}$$

$$r_{S_1} = \frac{\mu_1}{Y_{X/S,1}}\, X_{MT} \tag{5.15}$$

$$r_{S_2} = \frac{\mu_2 + \mu_3}{Y_{X/S,2}}\, (X_{MT} + X_{TK}) \tag{5.16}$$

$$r_P = (\mu_1 + \mu_2 + \mu_3)\, Y_{P/X}\, (X_{MT} + X_{TK}) \tag{5.17}$$

In the model μ_1 and μ_2 represent the specific growth rates of *M. thermoacetica* on xylose and glucose, respectively, while μ_3 denotes the specific growth rate of *T. kivui* on glucose. The parameter $\mu_{max,i}$ signifies the maximum growth rate of cells, with i indicating whether

Table 5.2: Parameters estimation for DMSO supplemented co-culture on DSM 60 medium containing glucose (12 g/L) and xylose (6 g/L).

Parameters					
R^2	0.81		$P_{m_{MT}}$	56.80 ± 0.08	g/L
MSE	0.30		$n_{P_{MT}}$	3.48 ± 0.46	
$\mu_{max,1}$	0.15 ± 0.003	h^{-1}	$\mu_{max,2}$	0.10 ± 0.03	h^{-1}
$K_{S,1}$	4.17 ± 0.17	g/L	$K_{S,2}$	15.90 ± 0.81	g/L
$S_{m,1}$	15.64 ± 0.14	g/L	$S_{m,2}$	136.10 ± 0.14	g/L
$n_{S,1}$	0.16 ± 0.08		$n_{S,2}$	0.001 ± 0.001	
$\mu_{max,3}$	0.11 ± 0.01	h^{-1}	K_{CCR}	0.002 ± 0.001	
$K_{S,3}$	0.66 ± 1.98	g/L	$Y_{X/S,1}$	0.29 ± 0.17	g/g
$P_{m_{TK}}$	34.77 ± 0.08	g/L	$Y_{X/S,2}$	0.26 ± 0.03	g/g
$n_{P_{TK}}$	1.03 ± 0.40		$Y_{P/X}$	1.47 ± 0.19	g/g

it pertains to *M. thermoacetica* on xylose (i=1), *M. thermoacetica* on glucose (i=2), or *T. kivui* on glucose (i=3). $K_{S,i}$ stands for the substrate saturation constant, P_m represents the maximum acetic acid concentration, and $S_{m,i}$ signifies the maximum concentration of substrate i.

Additionally, $Y_{X/S,i}$ denotes the cell yield concerning xylose and glucose, respectively, while $Y_{P/X}$ represents the overall product yield. The parameter K_{CCR} is associated with the carbon catabolite repression (CCR) mechanism.

In order to determine the unknown parameters, the differential equations were solved using Euler's first method in an Excel work spreadsheet and the MSE was minimized between the empirical and calculated values, represented by markers and solid lines, respectively, in Fig. 5.3.

The values of $\mu_{max,1}$, $K_{S,1}$, $S_{m,1}$, $n_{S,1}$, $\mu_{max,2}$, $K_{S,2}$, $S_{m,2}$, $n_{S,2}$, and K_{CCR} were deduced from substrate inhibition tests conducted on xylose and glucose for *M. thermoacetica*. $P_{m_{MT}}$ and $n_{P_{MT}}$ were acquired from product inhibition tests on *M. thermoacetica*. $\mu_{max,3}$ and $K_{S,3}$ were determined from the substrate inhibition tests on glucose for *T. kivui*. Finally $P_{m_{TK}}$ and $n_{P_{TK}}$ were obtained from product inhibition tests on *T. kivui*. Thus, the parameters subjected to optimization were the yields $Y_{X/S,1}$, $Y_{X/S,2}$, and $Y_{P/X}$ (Table 5.2).

Regrettably, the experiment did not include the determination of dry cell weight.

Therefore, a correlation between the DCW and OD_{600}, identified in the batch fermentation involving *M. thermoacetica* on both glucose and xylose substrates, was used:

$$DCW\ (g/L)\ =\ 0.3374\, OD_{600}\ -\ 0.044 \tag{5.18}$$

It's worth noting that this correlation may lack precision as it is based on data from a single bacterial strain.

The employed model, adapted from those utilized for single strains, and incorporating parameters derived from previous substrate and product inhibition tests for each bacterium, provides a good representation of the obtained results, albeit with limited precision. For a more precise examination, the ratio between the two microorganisms should have been continuously monitored throughout the fermentation process. Based on the sugar consumption trends, it is probable that up to 20 hours *T. kivui* was the dominant bacterium, while *M. thermoacetica* likely remained in the lag phase.

Chapter 6

Conclusions

To bring it all together, homoacetogenic microorganisms possess the unique ability to employ the WLP as the terminal electron sink in anabolism in addition to the carbon fixation pathway. The addition of the WLP as an isolated module to the conventional reactions of glucose fermentation via glycolysis theoretically enables the complete oxidation of one glucose molecule to three acetate molecules.

Two specific organisms, *Moorella thermoacetica* and *Thermoanaerobacter kivui*, were selected for experimentation due to their anaerobic and thermophilic nature, as well as the theoretical maximum yield achievable of 3 mol/mol using hexose sugars. The experiments were conducted using xylose and glucose, as they constitute a significant portion of lignocellulosic hydrolysates. These materials hold promise as non-food crop renewable resources, offering the potential for diverse product outputs such as transportation fuels, commodity chemicals, and high-value chemical precursors.

Moorella thermoacetica exhibits the unique capability of consuming xylose, which constitutes approximately 30-40% of lignocellulosic hydrolysates, albeit with greater inhibition compared to glucose. The Luong model effectively represents both single and dual-substrate inhibition in this strain. During the substrate inhibition test on xylose only, *M. thermoacetica* shows the highest yield of 1.56 mol/mol, with 76% of the initial 8.57 g/L of the pentose sugar consumed. Upon the simulatenous utilization of glucose and xylose, the strain exhibited an higher yield of 1.78 mol/mol, associated with the complete consumption of 3.84 g/L of xylose and 91% of the initial 6.57 g/L of glucose. In contrast, *Thermoanaerobacter kivui* thrives on glucose without discernible inhibition and does not utilize pentose sugars, requiring only the Monod model to represent its growth. The highest yield measured during the substrate inhibition test was 2.69 mol/mol, close

to the maximum theoretical yield, associated with the complete consumption of 8.86 g/L of glucose.

Both strains exhibit product inhibition, particularly due to acetate at pH greater than 6 and undissociated acetic acid at lower pH. In the product inhibition test, growth of both strains was completely inhibited by 0.58 M (34.3 g/L) of acetate.

Despite controlled pH and temperature, along with available substrate and ammonium-N, complete sugar consumption was not observed in any fermentation. When *M. thermoacetica* was grown on xylose, only 68% of the initial 16.27 g/L were consumed with a yield of 0.90 mol of acetic acid produced for mol of xylose consumed. However, more promising results were observed when the microorganism was provided with a combination of glucose and xylose. Here, 93% of the initial 5.45 g/L of xylose and 16% of the initial 10.87 g/L of glucose were consumed, resulting in a yield of 1.66 mol/mol based on the consumed sugars. *T. kivui* achieved an higher yield of 2.54 mol/mol, utilizing solely 46% of the initial 32.06 g/L of glucose.

In the fermentations growth ceased, likely indicating inhibition by an excess of reducing power. However, when the two strains were co-cultured, their performance improved upon the addition of dimethyl sulfoxide (DMSO) during the exponential phase. This addition facilitated the complete utilization of glucose and xylose in a 2:1 mass ratio, with 10.49 g/L of glucose and 5.34 g/L of xylose being fully consumed, yielding 1.28 mol/mol. Without the inclusion of DMSO, while 100% of the glucose was consumed, only 48% of the xylose underwent utilization.

These findings highlight a crucial aspect: the redox imbalance within the cells inhibits growth due to the cessation of the WLP, worsened by insufficient exogenous CO_2 supply. Future experiments should explore methods to enhance acetic acid yields by supplying CO_2, such as using higher concentrations of sodium bicarbonate, continuous liquid sparging, or working under higher pressure to increase dissolved CO_2 concentration. Thus, while these strains exhibit intriguing characteristics individually, their combined growth potential underscores the importance of optimizing environmental conditions for enhanced productivity.

Acknowledgments

All the experiments detailed in this thesis were conducted within the cutting-edge research infrastructure of VITO, the Flemish Institute for Technological Research, a leading European independent research organization dedicated to advancing sustainability and innovation. Nestled in Mol, Belgium, VITO specializes in a diverse array of scientific and technological domains, solidifying its position as a leading institution in environmental research, energy, materials, and beyond.

Bibliography

[1] J. R. Andreesen, A. Schaupp, C. Neurauter, A. Brown, L. G. Ljungdhal (1973) Fermentation of Glucose, Fructose, and Xylose by *Clostridium thermoaceticum*: Effect of Metals on Growth Yield, Enzymes, and the Synthesis of Acetate from CO_2. *Journal of Bacteriology, p. 743-751*

[2] N. Balasubramanian, J. S. Kim, Y. Y. Lee (2001) Fermentation of Xylose into Acetic Acid by *Clostridium thermoaceticum. Applied Biochemistry and Biotechnology, Vol. 91–93*

[3] M. Basen, V. Müller (2017) "Hot" acetogenesis. *Extremophiles, 21, p. 15–26*

[4] S. A. Braus-Stromeyer, G. Schnappauf, G. H. Braus, A. S. Goßner, H. L. Drake (1997) Carbonic Anhydrase in *Acetobacterium woodii* and Other Acetogenic Bacteria. *Journal of Bacteriology, p. 7197-7200*

[5] A. Chai, Y. Wong, S. Ong, N. A. Lutpi, S. Sam, W. Kee, H. Ng (2021) Haldane-Andrews substrate inhibition kinetics for pilot scale thermophilic anaerobic degradation of sugarcane vinasse. *Bioresource Technology, 336, 125319*

[6] G. Deshmukh, H. Manyar, "Production Pathways of Acetic Acid and Its Versatile Applications in the Food Industry", *Biotechnological Applications of Biomass*, IntechOpen, 2021

[7] H. Dette, V. B. Melas, A. Pepelyshev, N. Strigul (2005) Robust and efficient design of experiments for the Monod model. *Journal of Theoretical Biology, 234, p. 537–550*

[8] R. Domingues, M.Bondar, I.Palolo, O. Queirós, C. Dias de Almeida, M. T. Cesário (2021) Xylose Metabolism in Bacteria—Opportunities and Challenges towards Efficient Lignocellulosic Biomass-Based Biorefineries. *Applied Sciences, 11, 8112*

[9] H. L. Drake, S. L. Daniel (2004) Physiology of the thermophilic acetogen *Moorella thermoacetica*. *Research in Microbiology, 155, p. 422–436*

[10] H. L. Drake, A. S. Gobner, A. L. Daniel (2008) Old Acetogens, New Light. *Annals of the New York Academy of Sciences*

[11] M. Ehsanipour (2015) Bioconversion of lignocellulosic hydrolysate to acetic acid using *Moorella thermoacetica* [Master's thesis, University of Washington]

[12] M. Ehsanipour, A. V. Suko, R. Bura (2016) Fermentation of lignocellulosic sugars to acetic acid by *Moorella thermoacetica*. *Journal of Industrial Microbiology and Biotechnology, 43, p. 807–816*

[13] J. von Eysmondt, Dj. Vasic-Racki, Ch. Wandrey (1990) Acetic acid production by *Acetogenium kivui* in continuous culture - kinetic studies and computer simulations. *Applied Microbiology and Biotechnology 34:344-349*

[14] A. G. Fast, E. D. Schmidt, S. W Jones, B. P. Tracy (2015) Acetogenic mixotrophy: novel options for yield improvement in biofuels and biochemicals production. *Current Opinion in Biotechnology, 33:60–72*

[15] K. V. Gernaey, A. E. Lantz, P. Tufvesson, J. M. Woodley, G. Sin (2010) Application of mechanistic models to fermentation and biocatalysis for next-generation processes. *Trends in Biotechnology, 28, p.346–354*

[16] H. Huang, S. Wang, J. Moll, R. K. Thauera (2012) Electron Bifurcation Involved in the Energy Metabolism of the Acetogenic Bacterium *Moorella thermoacetica* Growing on Glucose or H_2 plus CO_2. *Journal of Bacteriology p. 3689–3699*

[17] S. C. Karekar, K. Srinivas, B. K. Ahring (2019) Kinetic Study on Heterotrophic Growth of *Acetobacterium woodii* on Lignocellulosic Substrates. *Fermentation, 5, 17*

[18] S. C. Karekar, R. Stefanini, B. K. Ahring (2022) Homo-Acetogens: Their Metabolism and Competitive Relationship with Hydrogenotrophic Methanogens. *Microorganisms, 10, 397*

[19] A. Katsyv, S. Jain, M. Basen, V. Müller (2021) Electron carriers involved in autotrophic and heterotrophic acetogenesis in the thermophilic bacterium *Thermoanaerobacter kivui*. *Extremophiles, 25, p. 513–526*

[20] R. Kellum, H. L. Drake (1984) Effects of Cultivation Gas Phase on Hydrogenase of the Acetogen *Clostridium thermoaceticum*. *Journal of Bacteriology, p. 466-469*

[21] R. Klemps, S. M. Schoberth, H. Sahm (1987) Production of acetic acid by *Acetogenium kivui*. *Applied Microbiology and Biotechnology 27:229—234*

[22] S. Kobayashi, J. Kato, K. Wada, K. Takemura, S. Kato, T. Fujii, Y. Iwasaki, Y. Aoi, T. Morita, A. Matsushika, K. Murakami, Y. Nakashimada (2022) Reversible Hydrogenase Activity Confers Flexibility to Balance Intracellular Redox in *Moorella thermoacetica*. *Frontiers in Microbiology, Volume 13, Article 897066*

[23] R. A. Kohn, T. F. Dunlap (1998) Calculation of the Buffering Capacity of Bicarbonate in the Rumen and In Vitro. *Journal of Animal Science, 76:1702–1709*

[24] Y. J. Kwon, C. R. Engler (2005) Kinetic Models for Growth and Product Formation on Multiple Substrates. *Biotechnology and Bioprocess Engineering 10: 587-592*

[25] J. A. Leigh, F. Mayer, R. S. Wolfe (1981) *Acetogenium kivui*, a New Thermophilic Hydrogen-Oxidizing, Acetogenic Bacterium. *Archives of Microbiology 129:275-280*

[26] S. Liu, "Kinetic Theory and Reaction Kinetics", "How cells grow", "Cell cultivation" *Bioprocess Engineering, 2^{nd} edition*, Elsevier, 2017, p. 259-287, 629-691, 700-705

[27] L. Lundie, H. Drake (1984) Development of a Minimally Defined Medium for the Acetogen *Clostridium thermoaceticum*. *Journal of OURNAL OF Bacteriology, Vo. 159, No. 2, p. 700-703*

[28] B. T. Maru, P. C. Munasinghe, H. Gilary, S. W. Jones, B. P. Tracy (2018) Fixation of CO_2 and CO on a diverse range of carbohydrates using anaerobic, non-photosynthetic mixotrophy. *FEMS Microbiology Letters, Vol. 365, No. 8*

[29] J. Monod (1949) The Growth of Bacterial Cultures. *Annual Review of Microbiology*

[30] J. Moon, S. Jain, V. Müller and M. Basen (2020) Homoacetogenic Conversion of Mannitol by the Thermophilic Acetogenic Bacterium *Thermoanaerobacter kivui* Requires External CO_2. *Frontiers in Microbiology, Volume 11*

[31] M. Muloiwa, S. Nyende-Byakika, M. Dinka (2020) Comparison of unstructured kinetic bacterial growth models. *South African Journal of Chemical Engineering, Vol. 33, p. 141-150*

[32] Y. Nakamura, H. Miyafuji, H. Kawamoto, S. Saka (2011) Acetic acid fermentability with *Clostridium thermoaceticum* and *Clostridium thermocellum* of standard compounds found in beech wood as produced in hot-compressed water. *The Japan Wood Research Society 57:331–337*

[33] M. D. Putra, A. E. Abasaeed (2018) A more generalized kinetic model for binary substrates fermentations. *Process Biochemistry 75, p. 31–38*

[34] S. W. Ragsdale, E. Pierce (2008) Acetogenesis and the Wood–Ljungdahl pathway of CO_2 fixation. *Biochimica et Biophysica Acta, 1784, p. 1873–1898*

[35] F. P. Rosenbaum, A. Poehlein, R. Daniel, V. Müller (2022) Energy-conserving dimethyl sulfoxide reduction in the acetogenic bacterium *Moorella thermoacetica*. *Environmental Microbiology, 24(4), p. 2000–2012*

[36] F. P. Rosenbaum, V. Müller (2023) *Moorella thermoacetica*: A promising cytochrome- and quinone-containing acetogenic bacterium as platform for a CO_2-based bioeconomy. *Green Carbon, 1, p.2–13*

[37] G. Rosero-Chasoy, R. M. Rodríguez-Jasso, C.N. Aguilar, G. Buitrón, I. Chairez, H. A. Ruiz (2021) Microbial co-culturing strategies for the production high value compounds, a reliable framework towards sustainable biorefinery implementation – an overview. *Bioresource Technology, 321, 124458*

[38] E. Schmitt, R. Bura, R. Gustafson, M. Ehsanipour (2016) Kinetic modeling of *Moorella thermoacetica* growth on single and dual-substrate systems. *Bioprocess and Biosysteme Engineering 39:1567–1575*

[39] K. Schuchmann, V. Müller (2016) Energetics and Application of Heterotrophy in Acetogenic Bacteria. *Applied and Environmental Microbiology, Volume 82, Number 14*

[40] R. D. Schwartz, F. A. Keller (1982) Acetic Acid Production by *Clostridium thermoaceticum* in pH Controlled Batch Fermentations at Acidic pH. *Applied and Environmental Microbiology, Vol. 43, No. 6, p. 1385-1392*

[41] S. M. Scully, J. Orlygsson, "Cultivation Techniques and Molecular Methods of Identification of Thermophilic, Anaerobic Bacteria", *Thermophilic Anaerobes*, Springer, 2023, p.109-129

[42] K. Sugaya, D. Tuse, J. L. Jones (1986) Production of Acetic Acid by *Clostridium thermoaceticum* in Batch and Continuous Fermentations. *Biotechnology and Bioengineering, Vol. XXVIII, p. 678-683*

[43] L. H. Smith, P. K. Kitanidis, P. L. McCarty (1997) Numerical Modeling and Uncertainties in Rate Coefficients for Methane Utilization and TCE Cometabolism by a Methane-Oxidizing Mixed Culture. *Biotechnology and Bioengineering, Vol. 53, No. 3*

[44] Statista Research Department, Jul 11, 2023. *Market volume of acetic acid worldwide from 2015 to 2022, with a forecast for 2023 to 2030.* Accessed October 31, 2023 *https://www.statista.com/statistics/1245203/acetic-acid-market-volume-worldwide/*

[45] Statista Research Department, Jul 11, 2023. *Global sulfuric acid market volume 2015-2030* Accessed November 17, 2023 *https://www.statista.com/statistics/1245226/sulfuric-acid-market-volume-worldwide/*

[46] A. J.J. Straathof (2023) Modelling of end-product inhibition in fermentation. *Biochemical Engineering Journal, 191, [108796]*

[47] G. Wang, D. I. C. Wang (1983) Elucidation of Growth Inhibition and Acetic Acid Production by *Clostridium thermoaceticum. Applied and Environmental Microbiology, Vol. 47, No. 2, p. 294-298*

[48] I. Yamamoto, T. Saikit, S. Liu, L. Ljungdahl (1983) Purification and Properties of NADP-dependent Formate Dehydrogenase from *Clostridium thermoaceticum*, a Tungsten-Selenium-Iron Protein. *Journal of Biological Chemistry, Vol. 258. No. 3, p. 1826-1832*